Review

Israel Journal of Chemistry
www.ijc.wiley-vch.de

doi.org/10.1002/ijch.202300181

N^6-methyladenosine in Mammalian Messenger RNA: Function, Location, and Quantitation

Ruiqi Ge,[a, b, c] Mengshu Emily He,[a, b] and Weixin Tang*[a, b]

Abstract: N^6-methyladenosine (m^6A) is the most abundant internal modification in mammalian messenger RNA (mRNA), constituting 0.1%–0.4% of total adenosine residues in the transcriptome. m^6A regulates mRNA stability and translation, pre-mRNA splicing, miRNA biogenesis, lncRNA binding, and many other physiological and pathological processes. While the majority of m^6As occur in a consensus motif of DRm^6ACH (D=A/G/U, R=A/G, H=U/A/C), the presence of such a motif does not guarantee methylation. Different RNA copies transcribed from the same gene may be methylated to varying levels. Within a single transcript, m^6As are not evenly distributed, showing an enrichment in long internal and terminal exons. These characteristics of m^6A deposition call for sequencing methods that not only pinpoint m^6A sites at base resolution, but also quantitate the abundance of methylation across different RNA copies. In this review, we summarize existing m^6A profiling methods, with an emphasis on next generation sequencing-(NGS−)based, site-specific, and quantitative methods, as well as several emerging single-cell methods.

1. Introduction

1.1 Brief Introduction to RNA Modifications

Nucleic acids – DNA and RNA – are fundamental to life. They are essentially biopolymers assembled from four types of nucleotides: deoxyadenosine (dA), deoxycytidine (dC), deoxyguanosine (dG), deoxythymidine (dT) for DNA, and adenosine (A), cytidine (C), guanosine (G), uridine (U) for RNA. Apart from the genetic information they encode, nucleotides contain certain moieties that could be reacted with, either chemically or biochemically, to yield modified nucleotides. The first naturally occurring modified nucleotide discovered, 5-methyl-2'-deoxycytidine (5mdC), was detected in the DNA from calf thymus extract via paper chromatography in 1948.[1] The first naturally occurring ribonucleotide modification, pseudouridine (Ψ), was discovered two years later.[2] Since then, more than 170 types of RNA modifications have been identified.[3–8] Technological advances, especially those in next-generation sequencing (NGS) and liquid chromatography-mass spectrometry (LC–MS), have promoted a resurgence of the field in recent years, enabling transcriptome-wide profiling of RNA modifications including N^6-methyladenosine (m^6A), N^6,2'-*O*-dimethyladenosine (m^6Am), 5-methylcytosine (m^5C), 5-hydroxymethylcytosine (hm^5C), inosine (I), pseudouridine (Ψ), N^1-methyladenosine (m^1A), 2'-*O*-methylation (Nm), N^4-acetylcytidine (ac^4C), N^7-methylguanosine (m^7G), and dihydrouridine (D).[3]

RNA modifications have been found in almost all RNA species. Transfer RNAs (tRNAs) are especially rich in modifications, hosting at least 111 types of modifications.[4] Eukaryotic tRNA molecules each contain 13 modified bases on average.[9] 33 types of modifications have been located in ribosomal RNAs (rRNAs).[8,9] Specifically, human rRNA contains 228 modifications of 14 different types.[10] In eukaryotes, mature messenger RNAs (mRNAs) carry a 5' cap, which is an m^7G modification appended to the 5' end of the first transcribed nucleotide via a triphosphate linker. Some cap structures contain further Nm modifications at the first one or two nucleotides, where the 2'-OH of the ribose is methylated to a 2'-*O*-methyl group (2'-OMe)[11,12] These modifications are essential for mRNA stability, splicing, polyadenylation, nuclear export, and cap-dependent translation.[12] Apart from Nm, internal mRNA modifications include m^6A, m^1A, m^5C, hm^5C, Ψ and at least 11 others[4–6] (Figure 1A). RNA modifications also occur in long non-coding RNAs (lncRNAs), microRNAs (miRNAs), piwi-interacting RNAs (piRNAs), small nuclear RNAs (snRNAs), small nucleolar RNAs (snoRNAs), and their corresponding precursors.[13]

1.2 m^6A: Distribution, Biochemistry, and Biological Functions

While Ψ is the most abundant RNA modification in general, m^6A is the most abundant internal mRNA modification in

[a] *R. Ge, M. E. He, W. Tang*
Department of Chemistry, The University of Chicago, Chicago, IL, USA
E-mail: weixintang@uchicago.edu
[b] *R. Ge, M. E. He, W. Tang*
Institute for Biophysical Dynamics, The University of Chicago, Chicago, IL, USA
[c] *R. Ge*
Program in Cellular and Molecular Medicine, Boston Children's Hospital, Boston, MA, USA

higher eukaryotes.[3–8] First discovered in 1974,[14] m^{6}A has been extensively investigated in the past decades.[6] From a chemistry point of view, m^{6}A is a simple *N*-monomethylation of the 6-amine of adenosine. Its counterpart in DNA, N^6-methyldeoxyadenosine (6mdA), is the predominant form of DNA methylation in prokaryotes.[15] Some viral RNAs were also found to contain m^{6}A, including human immunodeficiency virus-1 (HIV-1) genomic RNA.[16] m^{6}A is prevalent in the mammalian transcriptome: approximately 0.1-0.4% of total adenosines (m^{6}A/A) are N^6-methylated.[17] This also translates to 0.15–0.6% N^6-methylation of total adenosines in poly(A)$^+$ RNA, corresponding to 3–5 m^{6}A per transcript, 10–13 potential methylation sites per gene, or at least one m^{6}A in 25–60% of transcripts.[18–21] m^{6}A abundance varies among tissues and species, ranging from 0.11% to 0.23% m^{6}A/A in total RNA from human tissues, with urinary bladder being the lowest and skin being the highest. In mouse tissues the range was 0.10%–0.34%.[22] Non-coding RNAs also carry m^{6}A. Some lncRNAs are heavily methylated: X-inactive specific transcript (*XIST*), which is responsible for X-chromosome inactivation during mammalian development, contains at least 78 m^{6}A sites.[23] Metastasis associated lung adenocarcinoma transcript 1 (*MALAT1*), which is related to tumor metastasis and malignancy, contains at least 31 m^{6}A sites.[24] m^{6}A is also found in primary microRNAs (pri-miRNAs),[25] U6 snRNA,[26] snoRNAs, tRNAs, and rRNAs.[27] Human rRNA hosts 2 m^{6}A sites, one each in 18S rRNA and 28S rRNA.[10,28] Recent studies have revealed that retrotransposons, for example, long interspersed elements (LINE) 1, are also enriched in m^{6}A.[29–31]

Extensive studies have been conducted to elucidate the biochemistry of m^{6}A-related proteins, also known as "writers" (methyltransferases), "erasers" (demethylases), and "readers" (m^{6}A-binding proteins; Figure 1B). The m^{6}A methylation complex was first isolated from HeLa cells as 200 kDa and 875 kDa subcomplexes.[32] The core methyltransferase of the complex, methyltransferase-like 3 (METTL3) was first purified and characterized in 1994.[33,34] Wilms' tumor 1-associating protein (WTAP) was then discovered to be an important regulatory component of the complex.[35,36] METTL14, initially discovered via phylogenic analysis in comparison to METTL3 and thought to be an additional methyltransferase, was later proven to be an essential component forming heterodimeric complex with METTL3 yet catalytically deficient.[37–39] Vir-like m^{6}A methyltransferase associated protein (VIRMA, also known as KIAA1429),[40] RNA-binding motif protein 15/15B (RBM15/15B),[23] Cbl proto-oncogene like 1 (CBLL1, also known as Hakai), and zinc finger CCCH-type containing 13 (ZC3H13)[41–43] were further identified as key components of the ~1 MDa full complex. For non-coding RNAs, METTL16 was identified as the methyltransferase for U6 snRNA[44] and MAT2A pre-mRNA,[45] METTL5 for 18S rRNA,[46] and Zinc finger CCHC-type containing 4 (ZCCHC4) for 28S rRNA[47] (Figure 1C).

In 2011, the Chuan He group reported *in vitro* and *in vivo* demethylation of m^{6}A by fat mass and obesity-associated protein (FTO; Figure 1B),[48] a Fe (II)- and 2-oxoglutarate-dependent dioxygenases originally found to demethylate m^{3}dT/m^{3}U,[49] underscoring the potential dynamic regulation of m^{6}A. This inspired the concept of "RNA epigenetics"[50] or "epitranscriptomics"[51,52] that envisions dynamic and reversible regulation of RNA modifications in parallel to epigenetic regulation of DNA/histone modifications. m^{6}Am was later reported to be another substrate of FTO,[53,54] and alkB homolog 5 (ALKBH5) was identified as an additional m^{6}A demethylase (Figure 1B).[55] YT521-B homology (YTH) family proteins were among the first discovered and best studied m^{6}A-binding proteins in mammals. These include YTH N^6-methyladenosine RNA binding protein (YTHDF) 1–3 and YTH domain containing proteins (YTHDC) 1,2.[23,56,57] The YTH domain consists of 100–150 amino acid residues, with 4–5 alpha helices surrounding a curved six-stranded beta sheet.[58] YTHDF paralogs are highly conserved cytosolic

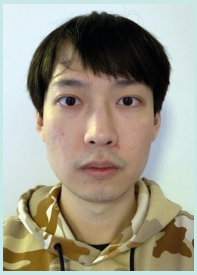

Ruiqi Ge obtained his B.S. from Peking University. He then obtained his Ph.D. in Chemistry in 2023 under the supervision of Prof. Chuan He at the University of Chicago. His research was focused on site-specific and quantitative sequencing of m^{6}A. He is currently a post-doctoral research fellow in Boston Children's Hospital under the supervision of Prof. Yi Zhang, studying hematopoietic stem and progenitor cells.

Mengshu Emily He received her B.S. in Biochemistry from University of Michigan. She is currently a fourth-year Chemistry Ph. D. candidate in the Weixin Tang lab focusing on m^{6}A detection methods using next-generation sequencing.

Weixin Tang received her B.S. in Chemistry and Biology from Tsinghua University and her Ph.D. in Chemistry from the University of Illinois, Urbana-Champaign. She was a Jane Coffin Childs Memorial postdoctoral fellow at the Broad Institute of MIT and Harvard prior to joining the Chemistry Department at the University of Chicago as a Neubauer Family Assistant Professor in 2019. The Tang Lab works towards a comprehensive toolbox for precise manipulation of the human genome, and for detecting epigenetic and epitranscriptomic modifications at high resolution.

Israel Journal of Chemistry

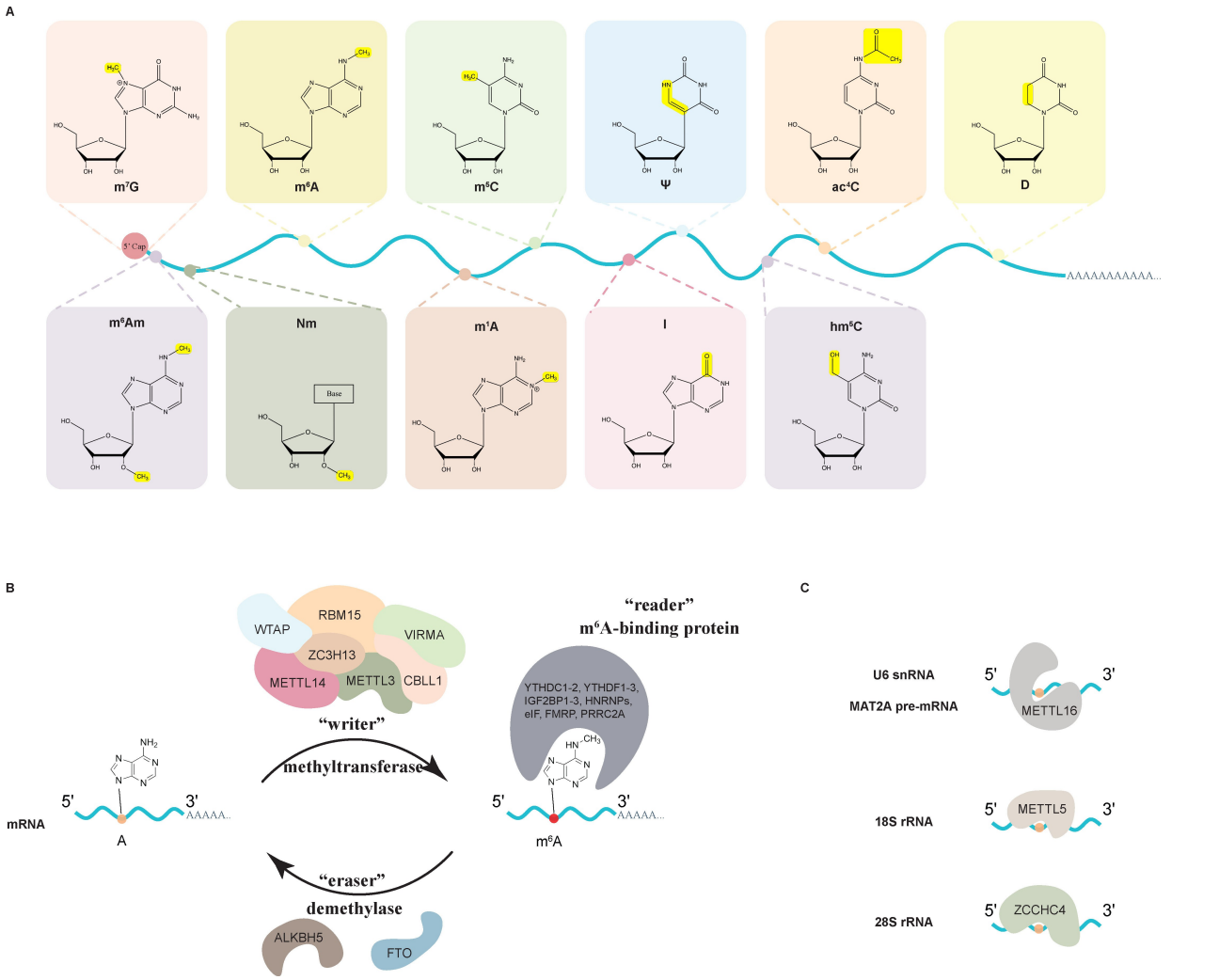

Figure 1. Common modifications in mammalian mRNA. **A**. common post-translational modifications mammalian mRNA. m^{7}G, *N*^{7}-methylguanosine; m^{6}A, *N*^{6}-methyladenosine; m^{5}C, 5-methylcytosine; Ψ, pseudouridine; ac^{4}C, *N*^{4}-acetylcytidine; D, dihydrouridine; Nm, 2'-*O*-methylation; m^{6}Am, *N*^{6},2'-*O*-dimethyladenosine; m^{1}A, *N*^{1}-methyladenosine; I, inosine; hm^{5}C, 5-hydroxymethylcytosine. **B**. Schematic representation of the dynamic interplay between m^{6}A writers, erasers, and readers. m^{6}A can be installed by the m^{6}A methylation complex ("writers"), removed by demethylases ("erasers"), and recognized by m^{6}A-binding proteins ("readers"). C. Other "writer" proteins responsible for m^{6}A installation in U6 snRNA, *MAT2A* pre-mRNA, 18S and 28S rRNA.

proteins, sharing about 85% sequence identity.[59] In addition to the conserved C-terminal YTH domain, they also contain an N-terminal intrinsically disordered region (IDR) which promotes phase-separation and stress granule formation.[60–64] On the contrary, YTHDC 1&2 bear less sequence homology to other YTH family proteins, and YTHDC1 is the only nuclear localized protein of the five.[54,57,65] Other identified m^{6}A-binding proteins outside of the YTH family include insulin-like growth factor 2 mRNA-binding proteins (IGF2BP) 1–3,[66] heterogeneous nuclear ribonucleoproteins (HNRNPs),[67–69] eukaryotic initiation factor (eIF) 3,[70] fragile X mental retardation protein (FMRP),[71,72] and proline rich coiled-coil 2 A (PRRC2A)[73] (Figure 1B).

Since its discovery, m^{6}A has been associated with various biological functions, including mRNA stability,[19,63,66,70,71,74–77] nuclear export,[72,78] translation,[63,64,66,79,80] pre-mRNA splicing,[45,67] miRNA biogenesis,[25,81] lncRNA binding,[23,82] etc. The most well-established function of m^{6}A is its negative impact on mRNA stability and promotion of mRNA turnover. Almost half a century ago, m^{6}A in the cytoplasm was already found to lose the radioactive label faster than the cap (m^{7}G), suggesting an m^{6}A-preferential degradation.[83] Subsequent comparison of mRNA half-life in *METTL3* knockdown (KD) cell lines versus control reaffirmed this observation.[40,74] Recently, multiple studies categorized all mRNA transcripts by their methylation loads through quantitative m^{6}A sequencing, which again showed strong negative correlation with their

half-lives.[84–86] Mechanistically, YTHDF2 was found to promote degradation of cytosolic mRNA by recruiting a deadenylation complex, CCR4-NOT, to methylated transcripts.[70] YTHDF1 was found to promote translation through interaction with translation initiation factors,[64] while YTHDF3 was reported to promote both translation and degradation possibly by interacting with YTHDF1 and YTHDF2.[63] Recent studies suggested that YTHDF1 also promotes degradation through interaction with argonaute RISC catalytic component (AGO) 2 and phase separation,[77] which underscores a plausible synergistic effect among the three YTHDF paralogs in accelerating mRNA turnover.[76] Intriguingly, in acute myeloid leukemia (AML)[66,87] and later in various other cancer cells,[88] studies showed that IGF2BPs, which are also m^{6}A-binding proteins, stabilized mRNAs they interact with.[65,86] These findings indicate that although in general m^{6}A stoichiometry is negatively correlated with mRNA stability, the downstream mechanism can be diverse and complex.

1.3 Physiological and Pathological Impact of m^{6}A

m^{6}A is intimately involved in physiological and pathological processes by regulating mRNA stability and processing. It forms an additional layer of regulation downstream to transcription that is programmed by transcription factors/chromatin states – the gene products associated with an mRNA molecule can either be down-regulated through YTHDF2-mediated degradation or up-regulated through YTHDF1,3-mediated translation initiation and IGF2BPs-mediated stabilization. For example, maternal mRNA clearance is required for the activation of zygotic genes to facilitate maternal-to-zygotic transition.[89] Such process was found to be m^{6}A-dependent, as knockout (KO) of *Ythdf2* in mice[90] and zebrafish[91] both resulted in developmental arrest. *Mettl3* KO, in contrast, is embryonically lethal in mice by embryonic day 5.5 (E5.5), while *Mettl3* KO mouse embryonic stem cells (mESCs) are viable yet do not differentiate.[92–94] Similar mechanisms also exist in endothelial-to-hematopoietic transition during hematopoietic stem cell (HSC) development in zebrafish.[95] m^{6}A was found to be important in the development of neuronal[96] and reproductive cells.[97,98] A recent study has demonstrated that transcripts of X-chromosomal genes are m^{6}A depleted compared to those of autosomal genes during early developmental stages, resulting in their longer half-lives and compensation for gene expression that is otherwise lost due to X-chromosome inactivation.[75]

m^{6}A has also been found to regulate immunity. The immune cells continue to proliferate and differentiate in adult organisms for maturation and activation of immune responses. Such processes involve large-scale transcriptomic and epigenomic remodeling, including co-regulation of the epitranscriptome, especially m^{6}A. m^{6}A-dependent regulation has been implied in both innate immunity and adaptive immunity. For example, macrophages can be polarized to either pro-inflammatory M1 or anti-inflammatory M2 subtypes via signaling from type I and type II cytokines, respectively. *Mettl3* KD in mouse bone marrow derived macrophages (BMDMs) significantly inhibited M1 polarization while enhancing M2 polarization. Mechanistically, methylation of signal transducer and activator of transcription 1 (*STAT*) mRNA was found to promote its translation, which favors M1 polarization.[99] For adaptive immunity, *Mettl3* conditional knockout (cKO) hindered the development of naïve T cells, by stabilizing mRNAs of suppressors of cytokine signaling (SOCS) family genes. Elevated SOCS protein levels inhibited interleukin (IL)-7/STAT5 signaling, which is important for T cell proliferation.[100] With a similar mechanism, CD4$^+$ regulatory T cell-(Treg-)specific *Mettl3* KO phenocopied systemic autoimmunity.[101] Some RNA viruses and retroviruses, for example, SARS-COV-2[102] and HIV-1,[103] harbor m^{6}A in their genomic RNA. A now Nobel-Prize winning study[104] revealed that such m^{6}A sites (along with other RNA modifications like pseudouridine) dampen Toll-like receptor (TLR)-mediated innate immune response against exogenous RNA, thereby facilitating viral infection.

Dysregulation of m^{6}A-related genes has pathological consequences. m^{6}A writers, readers, and erasers are recognized as tumor drivers or suppressors in a variety of cancers. In AML, METTL3, METTL14, METTL16, FTO, ALKBH5, YTHDF2, and IGF2BP2 are all overexpressed.[105] These up-regulation events concert in the overexpression of protooncogene *MYC* via two m^{6}A-dependent regulatory pathways: 1. FTO depletes m^{6}A in the first two exons of *MYC* mRNA, where YTHDF2 binds to promote degradation; 2. METTL3/14 preferentially increases m^{6}A in the last exon, where IGF2BP2 binds to stabilize.[105–107] This example highlights the multifaceted regulatory role of m^{6}A in gene expression. Alongside its functional implications in immunity, m^{6}A participates in the regulation of anti-tumor immunity and tumor microenvironments (TMEs). Transforming growth factor (TGF)-β, a TME-enriched cytokine, down-regulates METTL3 in natural killer (NK) cells. Such METTL3 deficiency decreases m^{6}A levels on Src homology region 2 domain-containing phosphatase-2 (SHP-2) transcripts, causing a reduction in their translation. This subsequently results in hyporeactivity of NK cells to IL-15 stimulation, inhibiting the anti-tumor activity of NK cells.[108] From a therapeutic perspective, researchers have developed METTL3 inhibitor STM2457 which stalls AML expansion both *in vitro* and *in vivo*.[109] A structurally different METTL3 inhibitor STM3006 was found to promote anti-tumor immunity, therefore active against both hematological and solid tumors. STM3006 was further optimized into STC-15 which is currently under Phase-I clinical trial for advanced solid tumors.[110]

m^{6}A-dependent regulation has been implicated in neuronal development and neurodegenerative diseases. m^{6}A levels in mouse brain increase drastically in adulthood compared to the embryo and neonate.[111] *Mettl14* cKO in embryonic mouse brains prolongs the cell cycle of radial glia cells and extends cortical neurogenesis into postnatal stages,[112] while cKO in

adult dorsal root ganglion (DRG) reduces functional axon regeneration in the peripheral nervous system.[113] As for neurodegenerative diseases, m^{6}A regulation has been strongly associated with Alzheimer's disease (AD).[114] In the brain tissue of AD patients, decreased expression levels of METTL3, METTL14, WTAP, FTO, and YTHDF1 result in m^{6}A reduction in large pyramidal neurons. On the contrary, microglia, the brain resident innate immune cells, experience m^{6}A level increase that contributes to neuroinflammation.[115] In an APP/PS1 mouse AD model, decreased Mettl3 expression is associated with an elevated level of phosphorylated tau protein (p-tau), which is hypothesized to be one of the causes of AD pathology. Conversely, overexpression of Mettl3 in the APP/PS1 mouse model promotes the autophagy of p-tau and alleviates hippocampal damage. Growing evidence also supports a regulatory role of m^{6}A in Parkinson's disease (PD).[116] The 6-hydroxydopamine-(6-OHDA-)induced rat PD model shows significant m^{6}A reduction in the striatum, with an up-regulation of Alkbh5.[117] The 1-methyl-4-phenyl-1,2,3,6-tetrahydropyridine-(MPTP-)induced mouse PD model experiences similar m^{6}A reduction with an up-regulation of Fto.[118] In both cases, *Fto* KD alleviates dopaminergic neuron death, a hallmark of PD. Additionally, translocated in liposarcoma/beta-catenin interacts with fusion (TLS/FUS), an RNA-binding protein (RBP) hypothesized to be a cause of amyotrophic lateral sclerosis (ALS), was found to bind strongly to m^{6}A and may therefore serve as a reader in the human HAP1 cell line.[119]

2. Biophysical Profiling of RNA Modifications

As mentioned in Section 1.1, pioneering studies of RNA modifications dated back to several decades ago. At that time, RNA modifications were profiled mostly based on their biophysical properties. Common techniques include radioactive isotope labeling, ion-exchange chromatography, affinity chromatography, two-dimensional thin layer chromatography (2D-TLC), and dot blot, in combination with nuclease digestion or selective chemical cleavage.[3,8]

Thin layer chromatography (TLC): TLC is a broadly used method for analytical and preparative separation of small-molecule mixtures. As an improvement over paper chromatography (which identified the first modified base 5mdC[1]), TLC utilizes a variety of stationary phases including silica gels, aluminum oxide, and cellulose to achieve differential retention of small molecules. The inherent differences in the analytes' chemical structures will affect both their solvation in the mobile phase and adsorption/desorption to the stationary phase, resulting in observable differences in the distance it travels normalized to the solvent front, known as the retention factor (Rf). For nucleotides, cellulose stationary phase is most commonly used. Separation could be further improved by expanding in two orthogonal directions, termed 2D-TLC. For example, m^{6}A and A can be distinguished in 2D-TLC using a solvent system consisting of isobutyric acid:0.5 M NH_4OH (5 : 3, v/v) in the first dimension and isopropanol:HCl:water (70 : 15 : 15, v/v/v) in the second dimension, with m^{6}A showing a higher Rf in both dimensions.[120,121] Although nucleotides could be visualized by UV absorption, the commonly used low-cost TLC visualization method, radioactive isotopic labeling using [^{32}P], [^{14}C], or [^{3}H] is often preferred due to its femtomol level sensitivity.[121,122] This method was once standard for tRNA modification analysis. When applied to rRNA, analysis becomes more difficult due to less frequent modifications.

High performance liquid chromatography (HPLC): Similar to TLC, liquid chromatography (LC) achieves separation of the analytes through differential partitioning between the mobile and stationary phase, resulting in different retention times (t_R). HPLC applies high pressure to the LC system (also implying smaller particles for the stationary phase), which significantly improves the resolution compared to gravity-driven LCs. At least three types of stationary phase materials are suitable for analyzing modified RNA nucleotides: reversed phase (RP), hydrophilic interaction (HILIC), and ion exchange (IEX). The separation relies on the differences in liquid-liquid partitioning, hydrophilic, hydrophobic, and electrostatic interactions between the analytes and the mobile/stationary phases. For example, the additional methyl group in m^{6}A increases its hydrophobicity, which translates to a longer t_R in RP-HPLC compared to A. Qualitative and quantitative analysis can be achieved using m^{6}A and A standards.

Some sequence information can be retained in these assays using sequence-specific nucleases. With a combination of nuclease P1, which promiscuously hydrolyzes all phosphodiester bonds; RNase A, which cleaves after pyrimidines; and RNase T1, which cleaves after guanosines, it is possible to further deduce the sequence context of the modification. RNase H, which cleaves the RNA strand of DNA: RNA hybrid, could be used with DNA probes to detect the modification in a sequence-specific manner. However, for RNA species longer than tRNA, it would be time consuming to sequence the modification sites solely by digestion and chromatography.

Mass spectrometry: Although purified m^{6}A and A can be well separated by TLC and HPLC, separation and quantification are difficult in a more complex biological context where analytes with a similar Rf/t_R would interfere. Technological advances in mass spectrometry (MS) have provided better tools. In mass spectrometry, molecules are ionized into gas-phase ions and analyzed by their corresponding mass-to-charge ratio (m/z). Except for pseudouridine versus uridine, all other RNA modifications form a mass shift compared to their unmodified counterparts. For example, m^{6}A would have a $+14$ shift in m/z compared to A due to the additional methyl group.

Many ionization methods have been developed for mass spectrometry.[123] The two most used for nucleic acids/nucleosides are: electron spray ionization (ESI)[124] and matrix assisted laser desorption/ionization (MALDI).[124] ESI can be readily used in tandem with HPLC to analyze both intact

oligonucleotides and nucleosides derived from digested nucleic acids, achieving high accuracy in identification and quantitation based on t_R, fragment m/z, and ion counts. MALDI can be used to ionize intact oligonucleotides without fragmentation, and modifications can be recognized from Δm/z of the whole molecule.

3. Site-Specific, Low-Throughput m^{6}A Profiling

A shared limitation of all previously described biophysical assays is their inability to precisely locate the modification within a transcript. Although RNase digestion could provide some information, the lack of sequence complexity in RNases A/T1 digestion and the labor-intensive procedure limit parallel analysis of multiple transcripts. Nevertheless, RNase H holds the promise for site-specific detection of modifications, in that the opposing DNA strand could be programmed to direct the cleavage site. Based on this principle, Liu *et al.* developed the SCARLET method.

Site-specific cleavage and radioactive-labeling followed by ligation-assisted extraction and thin-layer chromatography (SCARLET):[125] The cut site of RNase H in the target RNA can be programmed using a complementary 2'-OMe/2'-H chimeric oligonucleotide.[126,127] Specifically, cleavage will occur at the phosphodiester bond between the two ribonucleotides in the target RNA defined by the last 2'-OMe ribonucleotide and the first deoxyribonucleotide (2'-H) in the chimera. If the last 2'-OMe ribonucleotide in the probe is positioned at the very opposite to the modified ribonucleotide in the target, this cleavage will expose the modified ribonucleotide as the 5' end of the 3' half of the cleaved RNA. The resulting RNA fragments are subsequently dephosphorylated with calf intestine phosphatase (CIP), and rephosphorylated with T4 polynucleotide kinase (PNK) and γ-[^{32}P] ATP. Radioactively labeled fragments are isolated using polyacrylamide gel electrophoresis (PAGE), with ligation to increase the length to facilitate purification. Eventually the RNA fragments are digested to nucleotides by RNases A/T1 and nuclease P1 followed by 2D-TLC for modification identification.

The SCARLET method, albeit elegant, relies on biophysical properties of m^{6}A for detection, and is relatively labor-intensive. In 2018, Xiao *et al.* reported a protocol that also takes advantage of synthesized complementary probes, yet supports readout through quantitative polymerase chain reaction (qPCR).

Single-base elongation- and ligation-based PCR amplification (SELECT):[128] In SELECT, two DNA probes are designed complementary to the RNA target, with the assumed modified nucleotide skipped. Upon annealing, a DNA: RNA heteroduplex forms with only the modified base exposed. The single-nucleotide gap is then filled and ligated with *Bst* DNA polymerase and Chlorella virus-1 DNA ligase (commercialized as SplintR ligase). The presence of m^{6}A hinders both elongation and ligation, leading to higher quantification cycles (C_q) in the subsequent qPCR amplification of the ligated product. This method is facile and quantitative, serving as a standard verification method for some later studies.[85,129] However, as one would expect, for lowly methylated sites, changes in Cq (ΔCq) can be too minimal to be statistically significant.

Evolved TadA-assisted *N*^{6}-methyladenine sequencing (eTAM-seq):[86] This method relies on global deamination of A into inosine (I), while leaving m^{6}A unchanged. During reverse transcription (RT), I base pairs with C while m^{6}A pairs with T. The resulting cDNA, now carrying base conversion proportional to the A-to-m^{6}A ratio at all A sites, can be amplified with gene-specific primers and analyzed by Sanger sequencing or NGS. eTAM-seq is not only site-specific and quantitative, but also requires much less input compared to SCARLET and SELECT, supporting detection with as little as 250 pg of total RNA (~10 cells). Alternatively, eTAM-seq can be used for transcriptome-wide high-throughput profiling, which will be discussed in Section 5.

Although low-throughput assays typically require *a priori* knowledge of m^{6}A presence on target transcripts, they are more cost-effective, and the resulting information can be more readily associated with biological functions. Such prior knowledge can be obtained from *de novo* high-throughput profiling, which will be introduced in the following sections. Site-specific approaches are best suited for analyzing m^{6}A dynamics under perturbations, probing biological functions of known m^{6}A-bearing transcripts, and validating newly identified m^{6}A sites. From a diagnostic point of view, these methods are also suited for the evaluation of m^{6}A as a biomarker, especially eTAM-seq given its sensitivity. However, well-validated m^{6}A biomarkers have yet to be found, and further optimization of the workflow and cost of these methods may be needed for diagnostic applications.

4. Antibody-Based, High-Throughput m^{6}A Profiling

Initially used for genome sequencing, NGS was soon applied to transcriptomes, leading to the technology known as RNA sequencing (RNA-seq).[130,131] Modification sequencing can be achieved by enriching modification-bearing transcript fragments followed by RNA-seq.

Methylated RNA immunoprecipitation sequencing (MeRIP-seq)[111]**/m^{6}A-seq**:[56] RNA immunoprecipitation sequencing (RIP-seq)[132] is the tandem assay combining immunoprecipitation (IP) of RBP with RNA-seq. Using commercialized m^{6}A-specific antibodies, this method was extended to m^{6}A modification by two groups concurrently in 2012 (Figure 2A).[56,111] In addition to NGS, enriched RNAs can be analyzed by qPCR, where the enrichment over the IP input could be calculated from ΔCq and normalized against housekeeping genes (also known as the ΔΔCq method[133]), serving as a low-throughput version of MeRIP-seq known as MeRIP-qPCR.

Israel Journal of Chemistry

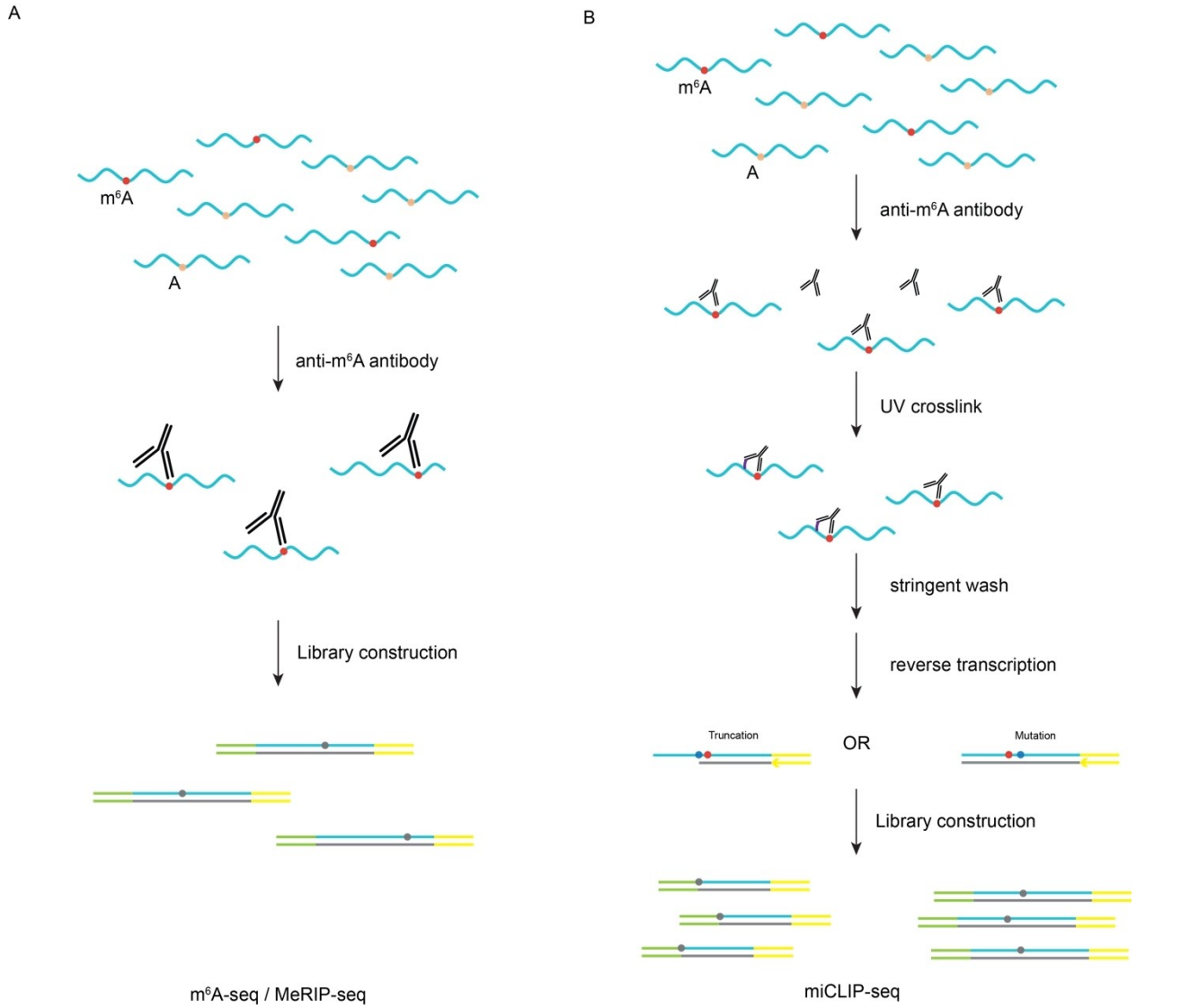

Figure 2. Antibody-based, high-throughput m^{6}A profiling methods. **A**. Schematic diagram of m^{6}A-seq/MeRIP-seq. Full-length or fragmented RNAs are enriched by anti-m^{6}A antibodies, and subsequently subjected to one of the many RNA-seq library construction protocols. **B**. Schematic diagram of miCLIP-seq. While also enriched by anti-m^{6}A antibodies similar to m^{6}A-seq, some m^{6}A adjacent RNA bases are now photo-crosslinked to proximal amino acid residues on the antibody. After digestion, crosslinked nucleobases can be readout as mismatches/deletions/truncations in RNA-seq.

A fragmentation step can be included prior to immunoprecipitation to narrow down the sequence segments that contain m^{6}A to a 100–200 bp window. The precise location of m^{6}A can be subsequently deduced from the m^{6}A consensus motif, DRm^{6}ACH (D = A/G/U, R = A/G, H = U/A/C).[21,27,52,54,57,65,134–136] Initially identified as Rm^{6}AC via nuclease digestion and chromatography,[137] the consensus sequence hosting m^{6}A was later refined to DRACH for *Homo sapiens* and *Mus musculus*, RRACH for *Arabidopsis thaliana*, and RGAC for *Saccharomyces cerevisiae*.[134] Pioneering work by the Chuan He group showed that both the METTL3/14 complex[38] and the YTH domain[74] bind preferentially to the consensus motif. However, within an MeRIP-seq peak (100–200 bp) there could be more than one DRACH motif, making assignment ambiguous. In fact, recent transcriptome-wide single-base resolution studies[84–86,138] found many more m^{6}A sites than previously anticipated.[19,129,139] In a 2023 paper by Uzonyi *et al.*,[19] the authors presented an *in silico* estimation of 3.4 m^{6}A per MeRIP "peak", which was reconstituted from predicted methylation sites. This signifies the limitation in resolution of m^{6}A-seq and MeRIP-seq.

m^{6}A individual-nucleotide-resolution cross-linking and immunoprecipitation sequencing (miCLIP-seq)[140]**/photo-crosslinking-assisted m^{6}A sequencing (PA-m^{6}A-seq)**:[141] As an effort to improve the site specificity of MeRIP-seq, miCLIP-seq and PA-m^{6}A-seq (Figure 2B) were developed

based on crosslinking and immunoprecipitation sequencing (CLIP-seq)[142] and photoactivatable ribonucleoside-enhanced crosslinking and immunoprecipitation (PAR-CLIP).[143] 254 nm ultraviolet (UV) light can induce free radical reactions between amino acid residues and RNA bases, forming a covalent bond if the two residues are physically close enough. Compared to native RIP, this crosslink stabilizes the interaction between RBP and its target, thus enabling stringent wash protocols to improve target specificity. Another advantage is that crosslinked amino acid residues can disrupt Watson-Crick base pairing, inducing mispairing (mutation), truncation (stop), or skipped bases (deletion) during RT. In the case of m^6A, such "RT signatures" could be used in conjunction with the DRACH motif in miCLIP-seq to deduce the precise location of the modification.

254 nm UV is considered energy-intensive for biomolecules, inducing undesirable non-specific crosslinks and chemical bond cleavages. By metabolically incorporating a UV-sensitive modified base, 4-thioluridine (4sU), CLIP reactions could be performed under 365 nm UV light. This method, known as PAR-CLIP, improves the specificity and crosslinking efficiency of canonical CLIP-seq. Given that GGACU is the most prominent motif among m^6A-hosting DRACH sequences,[134] the likelihood of having a U adjacent to m^6A is high, rendering PAR-CLIP particularly suited for m^6A detection (PA-m^6A-seq).

Despite their improved resolution, crosslinking-based methods have their own drawbacks. The 254 nm UV used in miCLIP-seq is prone to induce non-specific crosslinking and random mutations. Metabolic labeling, with limited 4sU incorporation frequencies, further lowers crosslinking and library construction efficiency. This also limits the application of PA-m^6A-seq to live cells, and to m^6A sites where an adjacent U is unavailable. Given its reduced sensitivity and transcriptome coverage, PA-m^6A-seq can be input demanding. Moreover, RNase T1 digestion combined with crosslink-induced RT stops typically generates shorter reads than standard RNA-seq. Shorter reads are more difficult to map to unique positions in the genome,[144] and the problem is exacerbated in the presence of mutations/stops/deletions. Due to these technical challenges, MeRIP-seq continues to be more popular than miCLIP-seq and PA-m^6A-seq.[145]

Antibody-based m^6A profiling strategies discussed above have two shared limitations: non-specific binding of the antibody[145–148] and the lack of stoichiometry information. Because antibodies are raised using synthetic moieties (known as haptens) attached to larger proteins for immunostimulation,[8] the recognition pattern for RNA strands will inevitably be different to some extent. An early study[148] published just one year after the initial MeRIP/m^6A-seq works estimated ~50% of the peaks to be false positives. An interesting feature of MeRIP/m^6A-seq data is its inclusion of ~25% of non-DRACH sites.[149] In the first paper reporting the m^6A consensus motif,[137] chromatography combined with RNase digestion and radioactive labeling revealed that apart from 70% GAC and 30% AAC, only "a very low amount" of radioactivity remained in other peaks. A later PAR-CLIP study revealed the preferential binding of METTL3, METTL14, and WTAP to the DRACH consensus sequence.[150] Given that later discovered methyltransferases, such as METTL16, METTL5, and ZCCHC4, only methylate a limited set of substrates (among these three, only METTL16 has a physiological mRNA substrate), non-DRACH sites are unlikely to be common, at least not in mRNA/poly(A)$^+$ RNA. Correspondingly, recent site-specific quantitative methods[84,86,138] reported much lower non-DRACH ratios. The high frequency of non-DRACH sites detected in MeRIP/m^6A-seq can be partially explained by the fact that anti-m^6A antibodies also bind to m^6Am. Indeed, m^6Am is estimated at 2.2–11.4% the abundance of m^6A[151] and resides in its own consensus motif of BCA (B = C/U/G).[151,152]

Additionally, variations in the pull-down efficiency and binding affinity to the antibody due to motifs and secondary structures[145] have prevented accurate quantitation of m^6A stoichiometry in antibody-dependent profiling methods. Why is stoichiometry a concern? Firstly, changes in m^6A levels may have a profound impact on biological functions, for example, mRNA half-life, as discussed in Section 1.2. Secondly, each m^6A site can harbor individual stoichiometry. In the pioneering paper reporting the m^6A consensus motif,[137] the authors estimated that with the assumption of each base sharing an equal appearance chance in the genome, the consensus motif of RACH should appear once per 43 nucleotides (1/2×1/4×1/4×3/4). Although m^6A is the most abundant internal mRNA modification, it is still rather scarce compared to this estimation. Based on MeRIP-seq results, approximately 5% of the DRACH motifs are methylated.[21] This could be an underestimation due to multiple m^6A sites present within each peak, or an overestimation due to incomplete methylation and false positives. This hypothesis is backed by MeRIP-qPCR and the quantitative low-throughput assays described in Section 4. Therefore, the biological information encoded by m^6A involves not only if an adenosine is methylated, but also the extent to which it is methylated, or stoichiometry.

Therefore, efforts have been made to upgrade the antibody-based m^6A profiling methods with better quantitation.

m^6A-level and isoform-characterization sequencing (m^6A-LAIC-seq):[153] One possible solution to m^6A stoichiometry quantitation is to simply divide the frequency of transcripts detected in the IP enriched sample by that of the IP input. To do so, normalization is required to account for variations in library preparation and sequencing. m^6A-LAIC-seq sought to introduce quantitation into MeRIP by spiking the ERCC (external RNA control consortium) control RNA mixes into the input, eluate, and supernatant fractions of an anti-m^6A immunoprecipitation assay. Because the ERCC pools should have the same read-out efficiency as their spike-in fractions, they can be used as an internal standard for normalization. Different from standard MeRIP, the authors used a saturating amount of antibody to ensure full quantitation. Their workflow also avoided fragmentation to differentiate between RNA isoforms. However, this approach remains semi-quantitative

due to the inherent variations in the IP efficiency. Its quantitation is on the transcript level, lacking distinction between different m^{6}A peaks within each transcript.

m^{6}A crosslinking exonuclease sequencing (m^{6}ACE-seq):[154] m^{6}ACE-seq sought to introduce quantitation into miCLIP-seq, by adding a 5' to 3' exonuclease (XRN1) digestion step after photo-crosslinking of m^{6}A to the anti-m^{6}A antibody. The exonuclease is blocked by crosslinked residues, and would therefore expose the crosslinked nucleotide at the start of the sequencing reads after decrosslinking and RT. m^{6}A stoichiometry can be calculated from the ratio of reads starting with an A and an undigested input control. This method is a significant improvement over miCLIP-seq, and stands among the earliest examples of site-specific and quantitative m^{6}A profiling. However, because of the inherent promiscuity of 254 nm photo-crosslinking and the difficulty in mapping read termini, typically due to random nucleotides added by the terminal deoxytransferase (TdT) domain of RT enzymes, identification and quantitation of m^{6}A sites with lower modification ratios tend to be less accurate.

Despite the aforementioned limitations, MeRIP-seq continues to be one of the most popular m^{6}A profiling methods. Compared to miCLIP-seq, PA-m^{6}A-seq, m^{6}A-LAIC-seq, m^{6}ACE-seq and more recent approaches to be introduced in the next section, MeRIP-seq employs a workflow that can be readily integrated into canonical RNA-seq assays. This means: 1. no hassle of preparing additional enzymes/chemicals, which can be demanding for researchers with no related background; 2. ease of applying commercially available RNA-seq kits, which typically boast easy-to-follow steps and well-tested protocols; 3. cost-effectiveness as reads are mostly allocated to enriched m^{6}A-bearing transcripts. Extensive optimization efforts have also been made to improve the overall efficiency and reduce sample amount requirement,[155] to develop algorithms that reduce technical variations when comparing different samples,[156] and to minimize antibody-specific artifacts by introducing modification-free controls.[157] MeRIP-seq together with other antibody-based approaches introduced in this section are best suited for transcriptome-wide analysis of m^{6}A dynamics under perturbations, *de novo* identification of m^{6}A methylated transcripts, and clinical studies involving large cohorts where cost-effectiveness considerations become inevitable.

5. Antibody-Free, High-Throughput m^{6}A Profiling

Limitations associated with antibody-dependent profiling methods have motivated the development of antibody-free approaches. How is m^{6}A different from an unmethylated A without being recognized as an antigen? Researchers sought to exploit the inherent chemical difference between these two structures. Enzymatic or chemical reactions capable of distinguishing m^{6}A from A, either by substrate selectivity or yielding chemically distinct products, can be harnessed for m^{6}A profiling. However, identifying candidate reactions can be challenging because the additional methyl group is small in size and chemically inert. Compounding challenges include an aqueous reaction environment to ensure the solubility of nucleic acids and incompatibility with strong bases or high temperature which would degrade the RNA.

FTO-assisted m^{6}A selective chemical labeling (m^{6}A-SEAL)[158]**/m^{6}A-label-seq**:[159] These two methods are antibody-free yet not quantitative. m^{6}A-SEAL utilizes intermediates of the FTO-catalyzed demethylation reaction for chemoenzymatic labeling of m^{6}A (Figure 3A). FTO, as a dioxygenase, demethylates the methylamine group by first oxidizing m^{6}A into N^6-hydroxylmethyladenosine (hm^{6}A), and then N^6-formyladenosine (f^{6}A). The *N*-formyl group will be hydrolyzed to N–H, thereby demethylating m^{6}A to A. The authors reacted hm^{6}A with dithiothreitol (DTT) to form N^6-dithiolsitolmethyladenosine, which contains a free thiol that could be further functionalized with thiol-reactive linkers (the authors used methanethiosulfonate) and biotin for pull-down enrichment. This method circumvents the antibody specificity issue yet does not support quantitation due to the use of pull-down enrichment.

m^{6}A-label-seq utilizes metabolic labeling to incorporate N^6-allyladenosine (a^{6}A) at physiological m^{6}A sites. METTL3/14, like other methyltransferases, use *S*-adenosyl methionine (SAM) as the methyl donor, with SAM being metabolically synthesized from methionine. In m^{6}A-label-seq, by feeding the cells with a chemically synthesized methionine analog, *Se*-allyl-L-selenohomocysteine, *Se*-allyl, *Se*-adenosylselenohomocysteine (allyl-SeAM) will be synthesized *in vivo* and used by METTL3/14 to transfer the allyl group to physiological m^{6}A sites. This transforms A to a^{6}A in place of m^{6}A, which could be further chemically derived with iodine to N^1,N^6-cyclized adenosine.[160] The cyclized product induces mispairing during RT with low-fidelity reverse transcriptases (HIV-1 RTase, for example). This method does not provide quantitation either, due to variations in metabolic labeling efficiency.

m^{6}A-sensitive RNA-endoribonuclease-facilitated sequencing (m^{6}A-REF-seq)[161]**/MAZTER-seq**:[162] Both methods take advantage of *Escherichia coli* RNA endonuclease MazF,[163] which digests ssRNA at the 5' of ACA sequence yet the cleavage is blocked by m^{6}ACA (Figure 3B). This feature allows for site-specific identification of m^{6}ACA and quantitation by counting the truncated reads versus total reads mapped to a given transcript. Using m^{6}A-REF-seq/MAZTER-seq, as many as 17,007 m^{6}A sites were identified from 100 ng of mRNA. The limitation of this method is apparent: m^{6}ACA is not prevalent among DRACH motifs. The authors' own estimation was that at most 16–25% of total m^{6}A can be detected. Like MeRIP-seq, this method could be adapted as a low-throughput verification method when combined with qPCR.

Deamination adjacent to RNA modification targets (DART-seq):[164] DART-seq utilizes the well-studied RNA C-to-U deaminase apolipoprotein B-editing enzyme, catalytic polypeptide-1 (APOBEC1), and exploits the fact that in DRACH there is always a C adjacent to m^{6}A (Figure 3C). In

Israel Journal of Chemistry

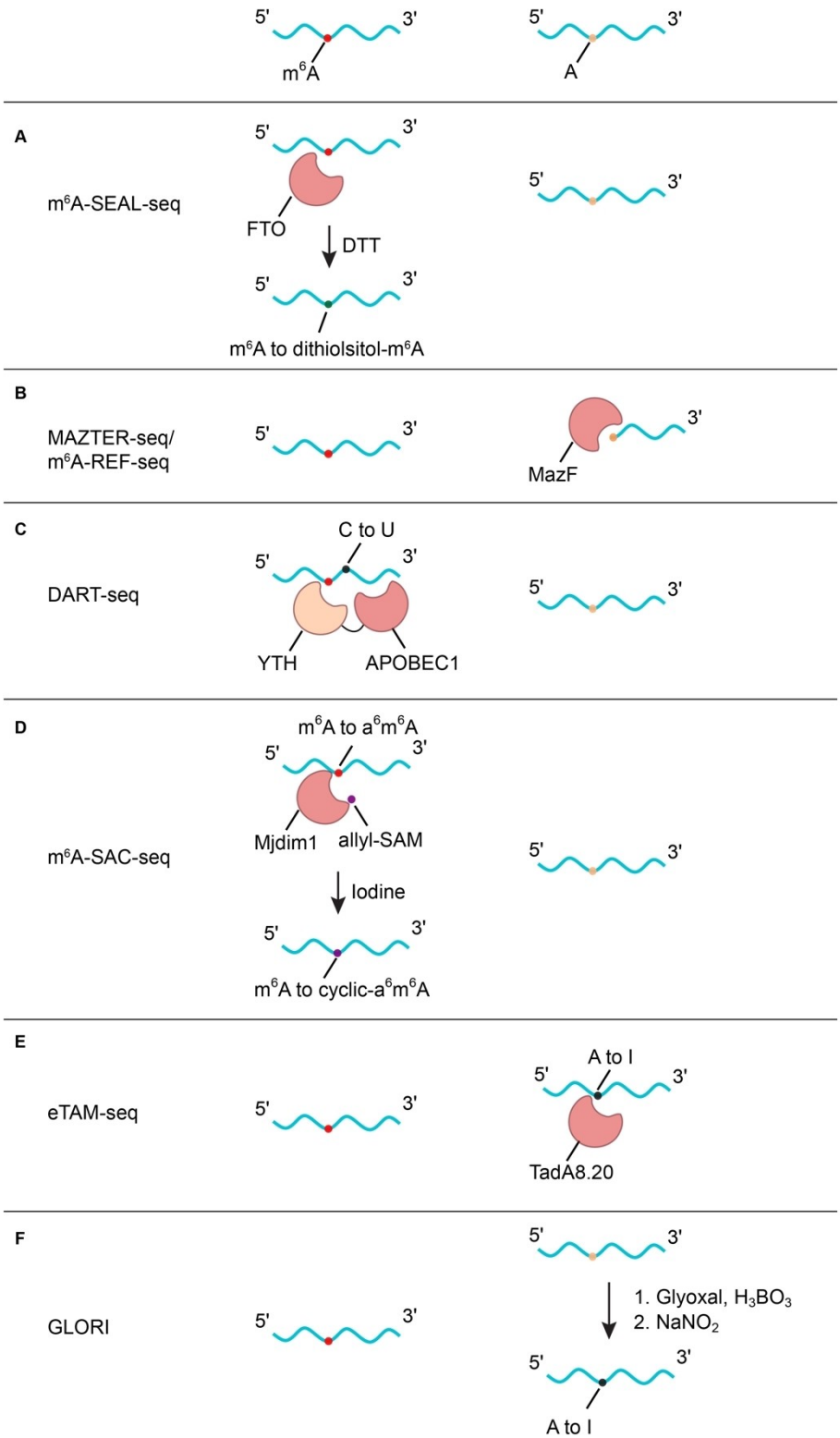

Figure 3. Antibody-free, high-throughput m^{6}A profiling methods. **A**. In m^{6}A-SEAL-seq, m^{6}A is selectively oxidized by FTO and then chemically labeled by DTT and thiol-reactive tags for pull-down enrichment. **B**. In MAZTER-seq/m^{6}A-REF-seq, MazF selectively cleaves the 5' phosphodiester bond of ACA, while such reaction is blocked by m^{6}ACA. **C**. In DART-seq, m^{6}A-adjacent C is deaminated to U via a APOBEC1-YTH fusion protein. **D**. In m^{6}A-SAC-seq, m^{6}A is functionalized with an additional allyl moiety by Mjdim1, which is subsequently chemically cyclized with iodine to generate a base-pair blocking structure that induces mismatch during RT. **E**. In eTAM-seq, A is selectively deaminated to I by TadA8.20, while leaving m^{6}A intact. **F**. In GLORI, A is chemically deaminated by $NaNO_2$, while leaving m^{6}A intact. Glyoxal and boric acid are added to form an adduct with G thus preventing it from being deaminated. The formed adducts are reversible. The second and third columns outline the chemical or enzymatic conversions that take place on m^{6}A and A, respectively.

DART-seq, APOBEC1 is genetically fused to an m^{6}A-binding YTH domain and overexpressed in cells. The deaminase is directed by the YTH domain to m^{6}A sites, where it catalyzes C-to-U conversion at the +1 C of m^{6}A. U base pairs with A during RT. m^{6}A sites can be inferred from a combination of the consensus motif and +1 C-to-U mutations. The strength of this method is that it does not involve any enzymatic or chemical treatment after cell lysis. Therefore, DART-seq could be used in tandem with advanced RNA-seq methods. This was elegantly demonstrated in **single-cell DART-seq** (**scDART-seq**),[165] where scRNA-seq technologies such as Smart-seq2[166] and commercialized 10x Genomics Next GEM 3'[167,168] were applied. DART-seq identified 12,672 m^{6}A sites with as low as 10 ng of total RNA, while scDART-seq captured 16,934 m^{6}A sites from 10,352 cells. The limitation of this method is that transfection/transduction is not always feasible for biological samples, such as frozen or formalin-fixed, paraffin-embedded (FFPE) tissue samples widely used in clinical studies. Overexpression of APOBEC1 may also result in off-target editing and unintended changes in cellular states. Although m^{6}A could be identified by the adjacency of mutated C in the DRACH motif, quantitation can be compromised due to the indirectness of the measurement.

m^{6}A-selective allyl chemical labeling and sequencing (m^{6}A-SAC-seq):[85] m^{6}A-SAC-seq (Figure 3D) was developed based on previous discoveries that *Methanocaldococcus jannaschii* dimethyltransferase 1 (Mjdim1) could convert m^{6}A into dimethyl A (m^{6,6}A),[169,170] and that iodine treatment of N^6-methyl, N^6-allyladenosine (m^{6}a^{6}A) generated an N^1-N^6 cyclized product which could be read out as a mismatch (predominantly A-to-T and A-to-C) during RT.[160] Although the conversion is not 100%, the methylation level can be calculated from the apparent mismatch ratio using linear regression of a series of internal standards with predefined methylation ratios. Despite using similar chemistry as m^{6}A-label-seq,[159] m^{6}A-SAC-seq offers three key advantages. 1. *In vitro* instead of metabolic labeling circumvents the labeling efficiency issue, therefore enabling accurate quantitation and improving sensitivity. 2. Metabolic labeling cannot be applied to frozen or FFPE tissue samples nor some demanding primary cells, while *in vitro* labeling is broadly applicable. 3. Cyclic-allyl-m^{6}A provides more steric hindrance than cyclic-allyl-A, which translates to a higher mutation ratio during RT and therefore improved sensitivity.

m^{6}A-SAC-seq uses the single-stranded ligation-based RNA-seq strategy, which is less efficient and more biased towards short reads[171] compared to contemporary template-switching-based RNA-seq strategies. Although mostly reserved for miRNA-seq now, optimization of such strategy[138] managed to accommodate longer reads. An optimized library construction workflow has significantly improved the profiling results of m^{6}A-SAC-seq, identifying 71,547 sites from 50 ng of mRNA or 31,233 sites from 2 ng of mRNA. Nevertheless, the intrinsic context bias of Mjdim1 limits the sensitivity of m^{6}A-SAC-seq against certain DRACH motifs (mostly AAC), a shortcoming that may be overcome by protein engineering.

eTAM-seq:[86] eTAM-seq was inspired by bisulfite sequencing,[172] which profiles 5-methylcytosine in DNA. In bisulfite sequencing, C is chemically deaminated while 5-methylcytosine retains, which could be read out as persistent C (unmutated). In eTAM-seq, m^{6}A profiling is enabled by deamination of A to I – which base pairs with C in the active site of polymerases[173] – while leaving m^{6}A intact (Figure 3E). Abundant modifications like m^{6}A can be readout as unmutated sites against the global A-to-G mutated background. Faithful detection demands efficient deamination of A (ideally to completion) coupled with high selectivity. *Escherichia coli* tRNA-specific adenosine deaminase (TadA) converts A to I in the single-stranded anticodon loop of tRNA^{Arg}. The potency and sequence compatibility of TadA have been increased by directed evolution,[174] with the TadA8 series showing the highest conversion efficiency.[175–177] These hyperactive TadA variants also have prefect selectivity for A over m^{6}A. The reaction condition was optimized for TadA8.20 to achieve 98.3% conversion of A regardless of the flanking sequence. The derived eTAM-seq workflow captured 69,834 m^{6}A sites in the HeLa transcriptome from 50 ng of mRNA.

eTAM-seq is quantitative given its robust A conversion regardless of the sequence context. Different from the modification-to-mutation paradigm demonstrated by m^{6}A-SAC-seq, the modification ratio is quantified as (1-mismatch %) in eTAM-seq.[85] The detected methylation ratios at well-studied sites, such as the non-coding RNA *MALAT1*, correlate well with the numbers reported previously by m^{6}A-SAC-seq and SCARLET. Since transcripts containing m^{6}A are not enriched, eTAM-seq requires a higher sequencing depth compared to conventional RNA-seq. With a slight modification in procedure, eTAM-seq also supports site-specific m^{6}A detection and quantification (detailed in Section 3).

Although initially demonstrated using single-stranded ligation-based RNA-seq, eTAM-seq is mechanistically compatible with most RNA-seq workflows including template-switching-based methods. Further optimization of the protocol as well as the deaminase might enable broader applications, for example, m^{6}A profiling in single cells.

Glyoxal and nitrite-mediated deamination of unmethylated adenosines (GLORI):[84] This method features chemical deamination of A to I while preserving m^{6}A (Figure 3F). Glyoxal, a highly reactive dialdehyde, reacts with the purine-amine of A and G via condensation reactions. Following oxidation by sodium nitrite ($NaNO_2$), the 6-amine of A will be converted to diazonium and subsequently hydrolyzed to hydroxyl, forming inosine (the enol tautomer). G, on the other hand, can be protected from oxidation with boric acid, and fully restored via heating at 95 °C for 10 min in an acidified formamide-water mixture. The conversion rate of this method is exceptionally high (>99%), which enables accurate quantitation of m^{6}A. Another advantage of the method lies in its low-cost and commercially available reagents. GLORI detected 176,642 sites in the HEK293T transcriptome from 200 ng of mRNA, more than 10-fold higher than what was reported with antibody-based methods.[19,114,126]

Antibody-free, site-specific, and quantitative sequencing methods represent the recent advances in m^{6}A profiling on the bulk level. Compared to MeRIP-seq, these methods offer an additional layer of information in precise location and stoichiometry. As previously discussed, both are important aspects of m^{6}A biology. The range of stoichiometry may indicate dynamic regulation of m^{6}A levels. Base-resolution detection is essential for designing site-specific perturbation through CRISPR-guided methyltransferases and demethylases.[178–180] Nevertheless, these methods typically involve customized RNA-seq workflows and preparation of delicate enzymes and chemicals. In the absence of enrichment, these assays also demand higher sequencing depths, especially for detecting low stoichiometric sites. Some of these assays have long protocols that take several days to complete, further hindering their applications in clinical labs. Commercialization of important assay components can significantly lower the barrier for adaptation.

Although these methods are free of antibody-related artifacts, they have their own drawbacks, such as off-target conversions due to the promiscuity of the enzymes/chemicals used and context-dependent variations in conversion rates. Some of the drawbacks can be overcome using modification-free controls,[157] or by upgrading the enzyme via protein engineering, as demonstrated by the latest advancement in the enzyme used for eTAM-seq.[181] At the current state, these assays are best suited for in-depth analysis of m^{6}A dynamics under perturbations and comprehensive *de novo* profiling of m^{6}A in unknown transcriptomes.

6. Single-Cell m^{6}A Profiling

scRNA-seq has been the most impactful development in RNA-seq over the past decade. Motivations for pursuing single-cell genomics/transcriptomics include limited sample availability and cell-to-cell heterogeneity. These considerations hold true for RNA modifications. For example, the m^{6}A stoichiometry measured by bulk profiling methods, as discussed in this review, could reflect either a uniform distribution within each cell or a statistical average of varying distribution patterns across the cell population. These scenarios could only be distinguished by single-cell or low-input m^{6}A profiling. Up to this date, four methods dedicated to this aim have been published.

Single-cell m^{6}A sequencing (scm^{6}A-seq):[182] As the name suggests, scm^{6}A-seq (Figure 4A) is derived from MeRIP-seq/m^{6}A-seq, the antibody-based m^{6}A profiling method. Mouse oocytes and blastomeres were collected in 96-well plates and lysed. RNA was fragmented and ligated to 3' adaptors, through which a hexamer sequence (cell barcode) unique to each cell was covalently appended to all RNA fragments. Barcoded RNAs from all cells were collected, mixed, and immunoprecipitated using anti-m^{6}A antibodies. Mouse rRNA was depleted using RNase H and complementary DNA probes. The remaining RNAs were reverse transcribed, and PCR amplified for sequencing. The authors demonstrated better classification of oocytes and blastomeres at different cell stages by overlaying scRNA-seq with scm^{6}A-seq data. They also recapitulated the asynchronous development of the two 2-cell blastomeres through changes observed in their RNA methylation profiles.

Picogram-scale m^{6}A RNA immunoprecipitation and sequencing (picoMeRIP-seq):[183] The authors carefully optimized the MeRIP-seq protocol to bring down the IP input from µg-scale RNA to picograms and eventually single zebrafish zygotes and mouse oocytes. The optimization was focused on improving the signal-to-noise ratio by implementing stringent washing conditions, using low-binding tubes, and choosing the most specific anti-m^{6}A antibody. The authors were able to achieve high reproducibility not only among replicates but also across input scales. They applied the method to mouse oocytes and early embryos, and identified 12,901 peaks per developmental stage. Unlike scm^{6}A-seq, these peaks allowed for cell-stage distinction without referring to RNA-seq. However, this picoMeRIP–seq workflow becomes more challenging when used in a multiplexed format and may not be applicable to smaller, differentiated single cells.

scDART-seq:[165] Already briefly introduced in Section 5, scDART-seq features the combination of DART-seq and advanced scRNA-seq techniques (Figure 4B), namely plate-based Smart-seq2[166] and droplet-based 10x Genomics Next GEM 3' methods.[167] scDART-seq uncovered sheer heterogeneity in the mRNA methylation profile in HeLa cells, where more than 80% of the m^{6}A sites only appear in 20% of the cells. To quote from the paper,[165] "while most mRNAs contain many total m^{6}A sites across all cells in the population, mRNAs are methylated at an average of only 1–3 sites in each cell, and individual sites are methylated in only 4.5% of cells on average".

Single-nucleus m^{6}A-CUT&Tag (sn-m^{6}A-CT):[184] This assay was developed based on single-cell CUT&TAG (sc-CT).[185] CUT&TAG,[186] an optimized version of CUT&RUN,[187] employs protein A–Tn5 transposase fusion protein (pA–Tn5) to transpose an adaptor sequence into DNA adjacent to antibody-defined targets, such as binding sites of histones or transcription factors (TFs). Using anti-m^{6}A antibodies in place of histone modification/TF antibodies, the authors demonstrated high-throughput single-cell m^{6}A profiling on non-genetically modified samples for the first time (Figure 4C). Of note, in sn-m^{6}A-CT, transposition was carried out on cDNA/RNA hybrids generated *in situ* via random-priming RT, rather than on dsDNA, the feasibility of which had been previously explored by other studies.[188,189] The authors also took advantage of the commercialized scATAC-seq/RNA-seq multiomics strategy[190,191] (essentially combining two sets of capturing sequences on the same beads) to generate an input reference of RNA expression for each cell, much like bulk m^{6}A-seq.

This study has provided intriguing insights into m^{6}A heterogeneity. Similar to sc-m^{6}A-seq, m^{6}A enrichment alone

Israel Journal of Chemistry

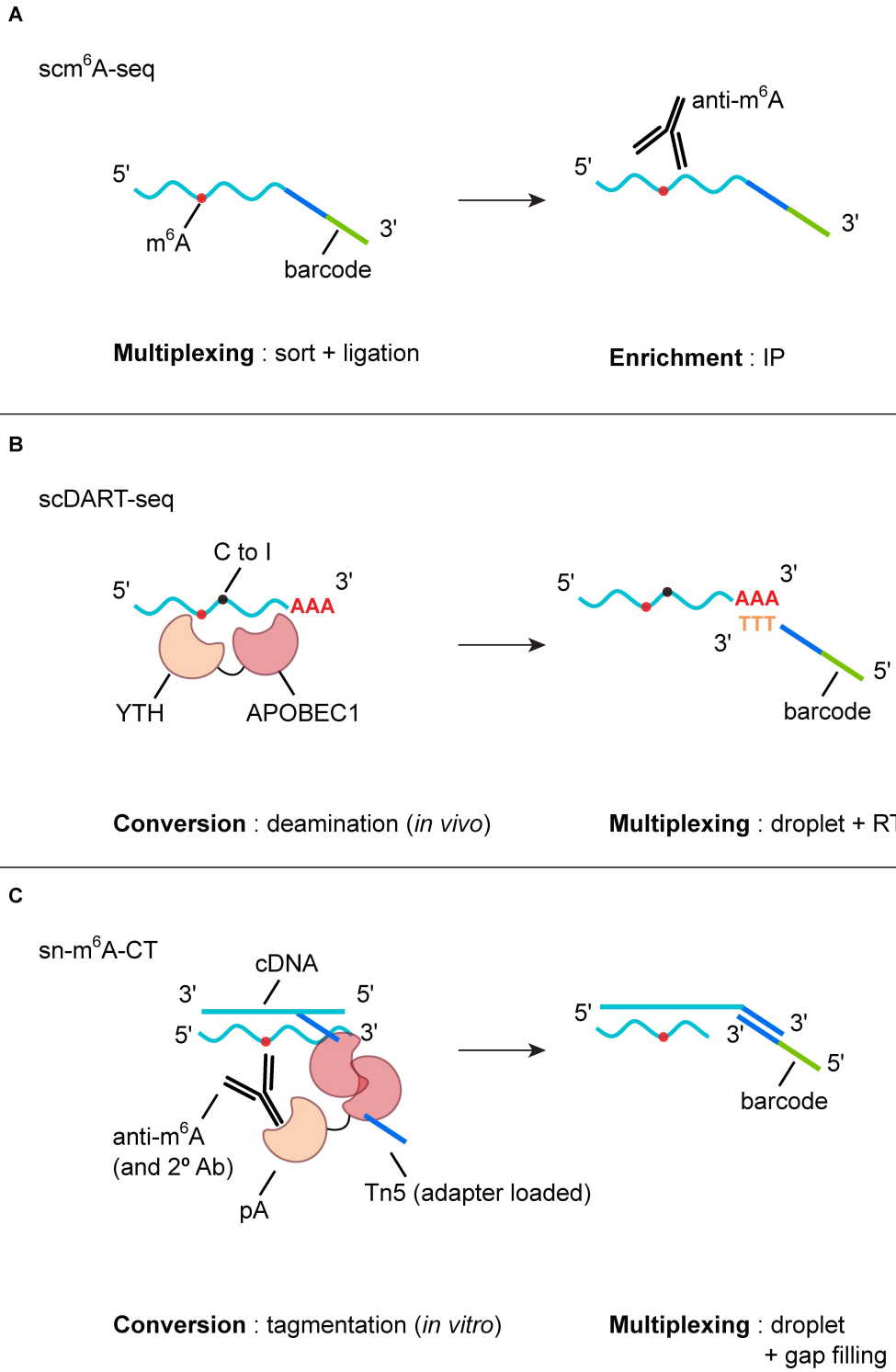

Figure 4. Multiplexing and conversion/enrichment strategies used for single-cell m^{6}A profiling. **A**. In scm^{6}A-seq, sorted single cells are individually ligated to barcoded adapters, thus keeping their identity in the subsequent pooled antibody enrichment. **B**. In scDART-seq, using the commercial workflow of 10x Genomics 3' scRNA-seq, the droplet-encapsulated single cells are annealed to gel bead-anchored, barcoded oligo-dT primers for template-switching RT. Labeling of m^{6}A adjacent C occurs *in vivo* prior to library construction. **C**. In sn-m^{6}A-seq, mRNAs in pooled cells (nuclei) were reverse transcribed using random primers and incubated with anti-m^{6}A antibodies, secondary antibodies (not shown here for simplicity), and pA–Tn5 for tagmentation, generating handle-attached cDNAs within each cell. Cells are individually encapsulated and gap-filled using a commercial 10x Genomics scATAC-seq/multiomics workflow. Gap-filling is enabled by annealing the handle to gel bead-anchored barcoded primers, which also achieves multiplexing. IP, immunoprecipitation. RT, reverse transcription. pA, protein A.

did not result in the identification of new cell clusters that were absent in scRNA-seq, but combining the two datasets did improve the contrast. Moreover, rare cell populations could harbor distinct m^{6}A features masked in bulk m^{6}A profiling. For example, the mouse expanded potential stem cells (EPSCs) contained a rare *Sox7*$^+$ population (3.2%) that was m^{6}A-modified on *Klb* mRNA, whereas the majority of *Sox7*$^-$ EPSCs were m^{6}A-depleted on *Klb* mRNA. This serves as an example that bulk m^{6}A profiling can overshadow globally scarce yet locally enriched m^{6}A modifications. The functional relevance of these locally enriched m^{6}A-modifications warrants further investigation.

Despite the exciting advances in single-cell studies, the field still awaits a broadly applicable, quantitative, base-resolution single-cell m^{6}A profiling method. This could be attributed to the difficulty of accommodating chemical/enzymatic conversions in droplet-based workflows. Advancements in combinatorial indexing and sample preservation have the potential to catalyze future breakthroughs. Multiple rounds of random barcoding can yield a pool of uniquely barcoded cells if the total number of combinations greatly exceeds the cell number. This idea was first implemented by **single-cell combinatorial indexing RNA sequencing (sci-RNA-seq)**,[192] where RT primer barcodes were combined with PCR primer barcodes, yielding 96×96 = 9216 combinations and expanding the capacity of plate-based scRNA-seq assays. The strength of this design was fully demonstrated in **split-pool ligation-based transcriptome sequencing (SPLiT-seq)**,[193] where RT primers were extended via splint ligation (a high efficiency ligation equivalent to nick sealing) for 3 rounds, and then combined with PCR primer barcodes. This yielded 96×96×96×24 = 21,233,664 combinations, which could uniquely label 1 million cells with high confidence, surpassing the upper limit of cell counts in droplet-based scRNA-seq. This workflow may also accommodate chemical/enzymatic conversions for modification detection. Nonetheless, full-length RNA in fixed cells might be challenging for enzymatic labeling and will require further optimization or innovation in labeling chemistry.

Much like the relationship between other bulk and single-cell sequencing technologies, single-cell m^{6}A profiling offers insight into its heterogeneity at the expense of sequencing quality (e.g., confident m^{6}A sites covered) and cost-effectiveness. While bulk assays have better sensitivity for low stoichiometric sites, single-cell assays excel at finding the subpopulation enriched of such modifications. The four single-cell methods introduced in this section are at their early stages and await future applications in systems of high heterogeneity, such as embryonic development, neuronal systems, hematopoietic systems, and tumor tissues.

7. A Glimpse at m^{6}A Profiling by Third-Generation Sequencing

Pioneering efforts have been made to detect RNA modifications by third-generation sequencing. A detailed comparison between third-generation sequencing and NGS is out of the scope of this article, and the readers are referred to a recent review article.[194] The key advantage of third-generation sequencing lies in its capability to sequence long reads covering the entire mRNA molecule. For m^{6}A, and RNA modifications in general, this would enable the profiling of *in-cis* regulation of multiple m^{6}A sites in the same transcript molecule. The cooperative or mutually exclusive presence of m^{6}A, information lost in short reads generated by NGS, is retained in third-generation sequencing.

Oxford Nanopore Technologies (ONT) have recently launched direct RNA sequencing (DRS).[195] The resulting data inherently contains modification information, because modified bases elicit shifts in current signals and affect the duration that nucleic acids reside in the pore (also known as dwell time).[196] These features could facilitate simultaneous, end-to-end profiling of various modifications. Currently two major directions are actively pursued: comparative and computational m^{6}A identification.

Comparative identification methods include detection of m^{6}A sites via direct RNA sequencing (DRUMMER),[197] Nanocompore,[198] epitranscriptional landscape inferring from glitches of ONT signals (ELIGOS),[199] and xPore.[200] These methods identify m^{6}A sites by comparing their signal shifts against a modification-free control. However, the inherent noises associated with ONT data may lead to potential false positive detection.

Alternatively, computational identification methods aim to predict m^{6}A sites using either NGS or ONT datasets to train machine learning models. These methods include EpiNano,[201] MINES,[202] nanom6A,[203] and m6Anet.[204] While EpiNano, MINES, and nanom6A use supervised learning, m6Anet is based on neural network algorithms. Although the accuracy of prediction is lower than comparative identification methods at the moment, more advances in this direction can be expected in the near future given the recent advances in machine learning.

8. Conclusions and Perspectives

Biophysical profiling of RNA modifications treats modified bases as small-molecule metabolites, which, although provided important early knowledge, failed to retain the site-specific stoichiometry information on modifications. Over the past decade, NGS-based methods have gradually become the preferred choice. NGS-based RNA-modification profiling can be viewed as specialized applications of RNA-seq, sharing many advances of the latter yet also facing unique challenges. The current best strategy is to convert modifications chemi-

cally or enzymatically into RNA-seq readable signals. The future direction of these methods will likely focus on improving the specificity, conversion efficiency, and ease of application, which includes considerations of cost, workflow robustness, and sample compatibility.

Many aspects of m^{6}A biology remains elusive, calling for further advancement in profiling methods. For example, the mechanism through which m^{6}A is selectively deposited among many DRACH motifs is not fully understood. Although recent findings on exon junction complex[19,129,139] indicate exclusion-dominant regulation, it is worth noting that m^{6}As in intronless transcripts of *S. cerevisiae* also show 3' UTR enrichment.[205] Expression and function of non-coding RNAs are also regulated by their m^{6}A levels. Non-poly(A)-based profiling methods are needed for dissecting the related processes, and a corresponding single-cell approach is necessary to fully understand the heterogeneity. In exploring pathology-related m^{6}A changes, a robust method capable of profiling FFPE samples on both bulk and single-cell levels should be established. In conclusion, innovations in detection technologies have profoundly advanced and will continue to advance our understanding of m^{6}A biology.

Author Contributions

E.M.H. and R.G. prepared the figures. R.G. and W.T. wrote the manuscript with input from E.M.H.

Acknowledgements

This work was supported by the Searle Scholars Program (SSP-2021-113), the Cancer Research Foundation Young Investigator Program, the American Cancer Society (RSG-22-043-01-ET), and the David & Lucile Packard Foundation (2022-74685).

Conflict of Interest

Authors declare no competing interests.

Data Availability Statement

Data sharing is not applicable to this article as no new data were created or analyzed in this study.

References

[1] R. D. Hotchkiss, *J. Biol. Chem.* **1948**, *175 (1)*, 315–332.
[2] W. E. Cohn, E. Volkin, *Nature* **1951**, *167 (4247)*, 483–484.
[3] Y. Zhang, L. Lu, X. Li, *Exp. Mol. Med.* **2022**, *54 (10)*, 1601–1616.
[4] P. J. McCown, A. Ruszkowska, C. N. Kunkler, K. Breger, J. P. Hulewicz, M. C. Wang, N. A. Springer, J. A. Brown, *Wiley Interdiscip. Rev. RNA*. **2020**, *11 (5)*, e1595.
[5] P. Boccaletto, F. Stefaniak, A. Ray, A. Cappannini, S. Mukherjee, E. Purta, M. Kurkowska, N. Shirvanizadeh, E. Destefanis, P. Groza, G. Avşar, A. Romitelli, P. Pir, E. Dassi, S. G. Conticello, F. Aguilo, J. M. Bujnicki, *Nucleic Acids Res.* **2022**, *50 (D1)*, D231–D235.
[6] V. A. Arzumanian, G. V. Dolgalev, I. Y. Kurbatov, O. I. Kiseleva, E. V. Poverennaya, *Int. J. Mol. Sci.* **2022**, *23 (22)*, 13851.
[7] S. Nachtergaele, C. He, *Annu. Rev. Genet.* **2018**, *52*, 349–372.
[8] M. Helm, Y. Motorin, *Nat. Rev. Genet.* **2017**, *18*, 275–291.
[9] I. A. Roundtree, M. E. Evans, T. Pan, C. He, *Cell.* **2017**, 1187–1200.
[10] M. Taoka, Y. Nobe, Y. Yamaki, K. Sato, H. Ishikawa, K. Izumikawa, Y. Yamauchi, K. Hirota, H. Nakayama, N. Takahashi, T. Isobe, *Nucleic Acids Res.* **2018**, *46 (18)*, 9289–9298.
[11] A. Ramanathan, G. B. Robb, S. H. Chan, *Nucleic Acids Res.* **2016**, *44 (16)*, 7511–7526.
[12] W. C. Merrick, *Gene.* **2004**, *332*, 1–11.
[13] X. Zhang, A. E. Cozen, Y. Liu, Q. Chen, T. M. Lowe, *Trends Mol. Med.* **2016**, *22 (12)*, 1025–1034.
[14] R. P. Perry, D. E. Kelley, *Cell* **1974**, *1 (1)*, 37–42.
[15] Z. K. O'Brown, E. L. Greer, *Adv. Exp. Med. Biol.* **2016**, *945*, 213–246.
[16] S. Chen, S. Kumar, C. E. Espada, N. Tirumuru, M. P. Cahill, L. Hu, C. He, L. Wu, *PLoS Pathog.* **2021**, *17 (3)*, e1009421.
[17] Y. Fu, C. He, *Curr. Opin. Chem. Biol.* **2012**, *16 (5-6)*, 516–524.
[18] I. A. Roundtree, M. E. Evans, T. Pan, C. He, *Cell.* **2017**, 1187–1200.
[19] A. Uzonyi, D. Dierks, R. Nir, O. S. Kwon, U. Toth, I. Barbosa, C. Burel, A. Brandis, W. Rossmanith, H. Le Hir, B. Slobodin, S. Schwartz, *Mol. Cell* **2023**, *83 (2)*, 237–251.e7.
[20] C. Liu, H. Sun, Y. Yi, W. Shen, K. Li, Y. Xiao, F. Li, Y. Li, Y. Hou, B. Lu, W. Liu, H. Meng, J. Peng, C. Yi, J. Wang, *Nat. Biotechnol.* **2023**, *41 (3)*, 355–366.
[21] P. C. He, C. He, *EMBO J.* **2021**, *40 (3)*, e105977.
[22] J. Liu, K. Li, J. Cai, M. Zhang, X. Zhang, X. Xiong, H. Meng, X. Xu, Z. Huang, J. Peng, J. Fan, C. Yi, *Mol. Cell* **2020**, *77 (2)*, 426–440.e6.
[23] D. P. Patil, C. K. Chen, B. F. Pickering, A. Chow, C. Jackson, M. Guttman, S. R. Jaffrey, *Nature* **2016**, *537 (7620)*, 369–373.
[24] X. Wang, C. Liu, S. Zhang, H. Yan, L. Zhang, A. Jiang, Y. Liu, Y. Feng, D. Li, Y. Guo, X. Hu, Y. Lin, P. Bu, D. Li, *Dev. Cell* **2021**, *56 (5)*, 702–715.e8.
[25] C. R. Alarcón, H. Lee, H. Goodarzi, N. Halberg, S. F. Tavazoie, *Nature* **2015**, *519 (7544)*, 482–485.
[26] K. E. Pendleton, B. Chen, K. Liu, O. V. Hunter, Y. Xie, B. P. Tu, N. K. Conrad, *Cell* **2017**, *169 (5)*, 824–835.e14.
[27] W. Huang, T. Q. Chen, K. Fang, Z. C. Zeng, H. Ye, Y. Q. Chen, *J. Hematol. Oncol.* **2021**, *14*, 117.
[28] B. E. H. Maden, *J. Mol. Biol.* **1986**, *189 (4)*, 681–699.
[29] J. Liu, M. Gao, J. He, K. Wu, S. Lin, L. Jin, Y. Chen, H. Liu, J. Shi, X. Wang, L. Chang, Y. Lin, Y.-L. Zhao, X. Zhang, M. Zhang, G.-Z. Luo, G. Wu, D. Pei, J. Wang, X. Bao, J. Chen, *Nature* **2021**, *591 (7849)*, 322–326.
[30] T. Chelmicki, E. Roger, A. Teissandier, M. Dura, L. Bonneville, S. Rucli, F. Dossin, C. Fouassier, S. Lameiras, D. Bourc'his, *Nature* **2021**, *591 (7849)*, 312–316.
[31] S.-Y. Hwang, H. Jung, S. Mun, S. Lee, K. Park, S. C. Baek, H. C. Moon, H. Kim, B. Kim, Y. Choi, Y.-H. Go, W. Tang, J.

Choi, J. K. Choi, H.-J. Cha, H. Y. Park, P. Liang, V. N. Kim, K. Han, K. Ahn, *Nat. Commun.* **2021**, *12 (1)*, 880.
[32] P. Narayan, F. M. Rottman, *Science (1979)* **1988**, *242 (4882)*, 1159–1162.
[33] J. A. Bokar, M. E. Rath-Shambaugh, R. Ludwiczak, P. Narayan, F. Rottman, *J. Biol. Chem.* **1994**, *269 (26)*, 17697–17704.
[34] J. A. Bokar, M. E. Shambaugh, D. Polayes, A. G. Matera, F. M. Rottman, *RNA* **1997**, *3 (11)*, 1233–1247.
[35] S. D. Agarwala, H. G. Blitzblau, A. Hochwagen, G. R. Fink, *PLoS Genet.* **2012**, *8 (6)*, e1002732.
[36] S. Zhong, H. Li, Z. Bodi, J. Button, L. Vespa, M. Herzog, R. G. Fray, *Plant Cell* **2008**, *20 (5)*, 1278–1288.
[37] X. Wang, J. Feng, Y. Xue, Z. Guan, D. Zhang, Z. Liu, Z. Gong, Q. Wang, J. Huang, C. Tang, T. Zou, P. Yin, *Nature* **2016**, *534* (7608), 575–578.
[38] J. Liu, Y. Yue, D. Han, X. Wang, Y. Fu, L. Zhang, G. Jia, M. Yu, Z. Lu, X. Deng, Q. Dai, W. Chen, C. He, *Nat. Chem. Biol.* **2014**, *10* (2), 93–95.
[39] P. Wang, K. A. Doxtader, Y. Nam, *Mol. Cell* **2016**, *63* (2), 306–317.
[40] S. Schwartz, M. R. Mumbach, M. Jovanovic, T. Wang, K. Maciag, G. G. Bushkin, P. Mertins, D. Ter-Ovanesyan, N. Habib, D. Cacchiarelli, N. E. Sanjana, E. Freinkman, M. E. Pacold, R. Satija, T. S. Mikkelsen, N. Hacohen, F. Zhang, S. A. Carr, E. S. Lander, A. Regev, *Cell Rep.* **2014**, *8* (1), 284–296.
[41] J. Wen, R. Lv, H. Ma, H. Shen, C. He, J. Wang, F. Jiao, H. Liu, P. Yang, L. Tan, F. Lan, Y. G. Shi, C. He, Y. Shi, J. Diao, *Mol. Cell* **2018**, *69* (6), 1028–1038.e6.
[42] C. Wan, B. Borgeson, S. Phanse, F. Tu, K. Drew, G. Clark, X. Xiong, O. Kagan, J. Kwan, A. Bezginov, K. Chessman, S. Pal, G. Cromar, O. Papoulas, Z. Ni, D. R. Boutz, S. Stoilova, P. C. Havugimana, X. Guo, R. H. Malty, M. Sarov, J. Greenblatt, M. Babu, W. B. Derry, E. R. Tillier, J. B. Wallingford, J. Parkinson, E. M. Marcotte, A. Emili, *Nature* **2015**, *525 (7569)*, 339–344.
[43] Y. Yue, J. Liu, J. Liu, X. Cui, J. Cao, G. Luo, Z. Zhang, T. Cheng, M. Gao, X. Shu, H. Ma, F. Wang, X. Wang, B. Shen, Y. Wang, X. Feng, C. He, J. Liu, *Cell Discov.* **2018**, *4*, 10.
[44] K. A. Doxtader, P. Wang, A. M. Scarborough, D. Seo, N. K. Conrad, Y. Nam, *Mol. Cell* **2018**, *71 (6)*, 1001–1011.e4.
[45] K. E. Pendleton, B. Chen, K. Liu, O. V. Hunter, Y. Xie, B. P. Tu, N. K. Conrad, *Cell* **2017**, *169 (5)*, 824–835.e14.
[46] N. van Tran, F. G. M. Ernst, B. R. Hawley, C. Zorbas, N. Ulryck, P. Hackert, K. E. Bohnsack, M. T. Bohnsack, S. R. Jaffrey, M. Graille, D. L. J. Lafontaine, *Nucleic Acids Res.* **2019**, *47 (15)*, 7719–7733.
[47] H. Ma, X. Wang, J. Cai, Q. Dai, S. K. Natchiar, R. Lv, K. Chen, Z. Lu, H. Chen, Y. G. Shi, F. Lan, J. Fan, B. P. Klaholz, T. Pan, Y. Shi, C. He, *Nat. Chem. Biol.* **2019**, *15 (1)*, 88–94.
[48] G. Jia, Y. Fu, X. Zhao, Q. Dai, G. Zheng, Y. Yang, C. Yi, T. Lindahl, T. Pan, Y. G. Yang, C. He, *Nat. Chem. Biol.* **2011**, *7 (12)*, 885–887.
[49] G. Jia, C.-G. Yang, S. Yang, X. Jian, C. Yi, Z. Zhou, C. He, *FEBS Lett.* **2008**, *582 (23–24)*, 3313–3319.
[50] C. He, *Nat. Chem. Biol.* **2010**, *6 (12)*, 863–865.
[51] Y. Saletore, K. Meyer, J. Korlach, I. D. Vilfan, S. Jaffrey, C. E. Mason, *Genome Biol.* **2012**, *13*, 175.
[52] D. Wiener, S. Schwartz, *Nat. Rev. Genet.* **2021**, *22(2)*, 119–131.
[53] J. Mauer, X. Luo, A. Blanjoie, X. Jiao, A. V. Grozhik, D. P. Patil, B. Linder, B. F. Pickering, J. J. Vasseur, Q. Chen, S. S. Gross, O. Elemento, F. Debart, M. Kiledjian, S. R. Jaffrey, *Nature* **2017**, *541 (7637)*, 371–375.
[54] K. D. Meyer, S. R- Jaffrey, *Annu. Rev. Cell Dev. Biol.* **2017**, *33*, 319–342.
[55] G. Zheng, J. A. Dahl, Y. Niu, P. Fedorcsak, C. M. Huang, C. J. Li, C. B. Vågbø, Y. Shi, W. L. Wang, S. H. Song, Z. Lu, R. P. G. Bosmans, Q. Dai, Y. J. Hao, X. Yang, W. M. Zhao, W. M. Tong, X. J. Wang, F. Bogdan, K. Furu, Y. Fu, G. Jia, X. Zhao, J. Liu, H. E. Krokan, A. Klungland, Y. G. Yang, C. He, *Mol. Cell* **2013**, *49 (1)*, 18–29.
[56] D. Dominissini, S. Moshitch-Moshkovitz, S. Schwartz, M. Salmon-Divon, L. Ungar, S. Osenberg, K. Cesarkas, J. Jacob-Hirsch, N. Amariglio, M. Kupiec, R. Sorek, G. Rechavi, *Nature* **2012**, *485 (7397)*, 201–206.
[57] D. Zhen, Y. Wu, Y. Zhang, K. Chen, B. Song, H. Xu, Y. Tang, Z. Wei, J. Meng, *Front. Cell Dev. Biol.* **2020**, *8*, 741.
[58] Z. Zhang, D. Theler, K. H. Kaminska, M. Hiller, P. de la Grange, R. Pudimat, I. Rafalska, B. Heinrich, J. M. Bujnicki, F. H.-T. Allain, S. Stamm, *J. Biol. Chem.* **2010**, *285 (19)*, 14701–14710.
[59] D. Hazra, C. Chapat, M. Graille, *Genes (Basel)* **2019**, *10 (1)*, 49.
[60] Y. Fu, X. Zhuang, *Nat. Chem. Biol.* **2020**, *16 (9)*, 955–963.
[61] Q. Fang, G. G. Tian, Q. Wang, M. Liu, L. He, S. Li, J. Wu, *Cell Rep.* **2023**, *42 (4)*, 112403.
[62] Y. Gao, G. Pei, D. Li, R. Li, Y. Shao, Q. C. Zhang, P. Li, *Cell Research* **2019**, *29 (9)*, 767–769.
[63] H. Shi, X. Wang, Z. Lu, B. S. Zhao, H. Ma, P. J. Hsu, C. Liu, C. He, *Cell Res* **2017**, *27 (3)*, 315–328.
[64] X. Wang, B. S. Zhao, I. A. Roundtree, Z. Lu, D. Han, H. Ma, X. Weng, K. Chen, H. Shi, C. He, *Cell* **2015**, *161 (6)*, 1388–1399.
[65] D. P. Patil, B. F. Pickering, S. R. Jaffrey, *Trends in Cell Biol.* **2018**, *28 (2)*, 113–127.
[66] H. Huang, H. Weng, W. Sun, X. Qin, H. Shi, H. Wu, B. S. Zhao, A. Mesquita, C. Liu, C. L. Yuan, Y.-C. Hu, S. Hüttelmaier, J. R. Skibbe, R. Su, X. Deng, L. Dong, M. Sun, C. Li, S. Nachtergaele, Y. Wang, C. Hu, K. Ferchen, K. D. Greis, X. Jiang, M. Wei, L. Qu, J.-L. Guan, C. He, J. Yang, J. Chen, *Nat. Cell Biol.* **2018**, *20* (3), 285–295.
[67] K. I. Zhou, H. Shi, R. Lyu, A. C. Wylder, Ż. Matuszek, J. N. Pan, C. He, M. Parisien, T. Pan, *Mol. Cell* **2019**, *76 (1)*, 70–81.e9.
[68] B. Wu, S. Su, D. P. Patil, H. Liu, J. Gan, S. R. Jaffrey, J. Ma, *Nat. Commun.* **2018**, *9 (1)*, 420.
[69] C. R. Alarcón, H. Goodarzi, H. Lee, X. Liu, S. Tavazoie, S. F. Tavazoie, *Cell* **2015**, *162 (6)*, 1299–1308.
[70] H. Du, Y. Zhao, J. He, Y. Zhang, H. Xi, M. Liu, J. Ma, L. Wu, *Nat. Commun.* **2016**, *7 (1)*, 12626.
[71] F. Zhang, Y. Kang, M. Wang, Y. Li, T. Xu, W. Yang, H. Song, H. Wu, Q. Shu, P. Jin, *Hum. Mol. Genet.* **2018**, *22 (15)*, 3936–3950.
[72] B. M. Edens, C. Vissers, J. Su, S. Arumugam, Z. Xu, H. Shi, N. Miller, F. Rojas Ringeling, G. Ming, C. He, H. Song, Y. C. Ma, *Cell Rep.* **2019**, *28 (4)*, 845–854.e5.
[73] R. Wu, A. Li, B. Sun, J.-G. Sun, J. Zhang, T. Zhang, Y. Chen, Y. Xiao, Y. Gao, Q. Zhang, J. Ma, X. Yang, Y. Liao, W.-Y. Lai, X. Qi, S. Wang, Y. Shu, H.-L. Wang, F. Wang, Y.-G. Yang, Z. Yuan, *Cell Res* **2019**, *29 (1)*, 23–41.
[74] X. Wang, Z. Lu, A. Gomez, G. C. Hon, Y. Yue, D. Han, Y. Fu, M. Parisien, Q. Dai, G. Jia, B. Ren, T. Pan, C. He, *Nature* **2014**, *505 (7481)*, 117–120.
[75] C. Rücklé, N. Körtel, M. F. Basilicata, A. Busch, Y. Zhou, P. Hoch-Kraft, K. Tretow, F. Kielisch, M. Bertin, M. Pradhan, M. Musheev, S. Schweiger, C. Niehrs, O. Rausch, K. Zarnack, C. I. Keller Valsecchi, J. König, *Nat. Struct. Mol. Biol.* **2023**, *30*, 1207–1215.
[76] S. Zaccara, S. R. Jaffrey, *Cell* **2020**, *181 (7)*, 1582–1595.e18.

[77] J. Li, K. Chen, X. Dong, Y. Xu, Q. Sun, H. Wang, Z. Chen, C. Liu, R. Liu, Z. Yang, X. Mei, R. Zhang, L. Chang, Z. Tian, J. Chen, K. Liang, C. He, M. Luo, *Cell Prolif.* **2022**, *55 (1)*, e13157.
[78] I. A. Roundtree, G.-Z. Luo, Z. Zhang, X. Wang, T. Zhou, Y. Cui, J. Sha, X. Huang, L. Guerrero, P. Xie, E. He, B. Shen, C. He, *eLife* **2017**, *6*, e31311.
[79] K. D. Meyer, D. P. Patil, J. Zhou, A. Zinoviev, M. A. Skabkin, O. Elemento, T. V. Pestova, S. B. Qian, S. R. Jaffrey, *Cell* **2015**, *163 (4)*, 999–1010.
[80] J. Choe, S. Lin, W. Zhang, Q. Liu, L. Wang, J. Ramirez-Moya, P. Du, W. Kim, S. Tang, P. Sliz, P. Santisteban, R. E. George, W. G. Richards, K. K. Wong, N. Locker, F. J. Slack, R. I. Gregory, *Nature* **2018**, *561 (7724)*, 556–560.
[81] Y. Gong, Q. Jiang, L. Liu, Q. Liao, J. Yu, Z. Xiang, X. Luo, *Physiol. Genomics* **2022**, *54 (9)*, 337–349.
[82] K. I. Zhou, M. Parisien, Q. Dai, N. Liu, L. Diatchenko, J. R. Sachleben, T. Pan, *J. Mol. Biol.* **2016**, *428 (5)*, 822–833.
[83] S. Sommer, U. Lavi, J. E. Darnell, *J. Mol. Biol.* **1978**, *124(3)*, 487–499.
[84] C. Liu, H. Sun, Y. Yi, W. Shen, K. Li, Y. Xiao, F. Li, Y. Li, Y. Hou, B. Lu, W. Liu, H. Meng, J. Peng, C. Yi, J. Wang, *Nat. Biotechnol.* **2023**, *41 (3)*, 355–366.
[85] L. Hu, S. Liu, Y. Peng, R. Ge, R. Su, C. Senevirathne, B. T. Harada, Q. Dai, J. Wei, L. Zhang, Z. Hao, L. Luo, H. Wang, Y. Wang, M. Luo, M. Chen, J. Chen, C. He, *Nat. Biotechnol.* **2022**, *40 (8)*, 1210–1219.
[86] Y. L. Xiao, S. Liu, R. Ge, Y. Wu, C. He, M. Chen, W. Tang, *Nat. Biotechnol.* **2023**, *41 (7)*, 993–1003.
[87] N. Zhang, Y. Shen, H. Li, Y. Chen, P. Zhang, S. Lou, J. Deng, *Exp. Mol. Med.* **2022**, *54 (2)*, 194–205.
[88] D. Ramesh-Kumar, S. Guil, *Semin. Cancer Biol.* **2022**, *86*, 18–31.
[89] K. N. Schulz, M. M. Harrison, *Nat. Rev. Genet.* **2019**, *20 (4)*, 221–234.
[90] I. Ivanova, C. Much, M. Di Giacomo, C. Azzi, M. Morgan, P. N. Moreira, J. Monahan, C. Carrieri, A. J. Enright, D. O'Carroll, *Mol. Cell* **2017**, *67 (6)*, 1059–1067.e4.
[91] B. S. Zhao, X. Wang, A. V. Beadell, Z. Lu, H. Shi, A. Kuuspalu, R. K. Ho, C. He, *Nature* **2017**, *542 (7642)*, 475–478.
[92] S. Geula, S. Moshitch-Moshkovitz, D. Dominissini, A. A. Mansour, N. Kol, M. Salmon-Divon, V. Hershkovitz, E. Peer, N. Mor, Y. S. Manor, M. S. Ben-Haim, E. Eyal, S. Yunger, Y. Pinto, D. A. Jaitin, S. Viukov, Y. Rais, V. Krupalnik, E. Chomsky, M. Zerbib, I. Maza, Y. Rechavi, R. Massarwa, S. Hanna, I. Amit, E. Y. Levanon, N. Amariglio, N. Stern-Ginossar, N. Novershtern, G. Rechavi, J. H. Hanna, *Science (1979)* **2015**, *347 (6225)*, 1002–1006.
[93] P. J. Batista, B. Molinie, J. Wang, K. Qu, J. Zhang, L. Li, D. M. Bouley, E. Lujan, B. Haddad, K. Daneshvar, A. C. Carter, R. A. Flynn, C. Zhou, K. S. Lim, P. Dedon, M. Wernig, A. C. Mullen, Y. Xing, C. C. Giallourakis, H. Y. Chang, *Cell Stem Cell* **2014**, *15 (6)*, 707–719.
[94] S. Ke, A. Pandya-Jones, Y. Saito, J. J. Fak, C. B. Vågbø, S. Geula, J. H. Hanna, D. L. Black, J. E. Darnell, R. B. Darnell, *Genes Dev.* **2017**, *31 (10)*, 990–1006.
[95] C. Zhang, Y. Chen, B. Sun, L. Wang, Y. Yang, D. Ma, J. Lv, J. Heng, Y. Ding, Y. Xue, X. Lu, W. Xiao, Y. G. Yang, F. Liu, *Nature* **2017**, *549 (7671)*, 273–276.
[96] K.-J. Yoon, F. R. Ringeling, C. Vissers, F. Jacob, M. Pokrass, D. Jimenez-Cyrus, Y. Su, N.-S. Kim, Y. Zhu, L. Zheng, S. Kim, X. Wang, L. C. Doré, P. Jin, S. Regot, X. Zhuang, S. Canzar, C. He, G. Ming, H. Song, *Cell* **2017**, *171 (4)*, 877–889.e17.
[97] H. Xia, C. Zhong, X. Wu, J. Chen, B. Tao, X. Xia, M. Shi, Z. Zhu, V. L. Trudeau, W. Hu, *Genetics* **2018**, *208 (2)*, 729–743.
[98] S.-T. Qi, J.-Y. Ma, Z.-B. Wang, L. Guo, Y. Hou, Q.-Y. Sun, *J. Biol. Chem.* **2016**, *291 (44)*, 23020–23026.
[99] Y. Liu, Z. Liu, H. Tang, Y. Shen, Z. Gong, N. Xie, X. Zhang, W. Wang, W. Kong, Y. Zhou, Y. Fu, *Am. J. Physiol. Cell Physiol.* **2019**, *317 (4)*, C762–C775.
[100] H.-B. Li, J. Tong, S. Zhu, P. J. Batista, E. E. Duffy, J. Zhao, W. Bailis, G. Cao, L. Kroehling, Y. Chen, G. Wang, J. P. Broughton, Y. G. Chen, Y. Kluger, M. D. Simon, H. Y. Chang, Z. Yin, R. A. Flavell, *Nature* **2017**, *548 (7667)*, 338–342.
[101] J. Tong, G. Cao, T. Zhang, E. Sefik, M. C. Amezcua Vesely, J. P. Broughton, S. Zhu, H. Li, B. Li, L. Chen, H. Y. Chang, B. Su, R. A. Flavell, H.-B. Li, *Cell Res* **2018**, *28 (2)*, 253–256.
[102] N. Li, H. Hui, B. Bray, G. M. Gonzalez, M. Zeller, K. G. Anderson, R. Knight, D. Smith, Y. Wang, A. F. Carlin, T. M. Rana, *Cell Rep.* **2021**, *35 (6)*, 109091.
[103] N. Tirumuru, B. S. Zhao, W. Lu, Z. Lu, C. He, L. Wu, *eLife* **2016**, *5*, e15528.
[104] K. Karikó, M. Buckstein, H. Ni, D. Weissman, *Immunity* **2005**, *23 (2)*, 165–175.
[105] X. Deng, Y. Qing, D. Horne, H. Huang, J. Chen, *Nat. Rev. Clin. Oncol.* **2023**, *20 (8)*, 507–526.
[106] X. Deng, R. Su, H. Weng, H. Huang, Z. Li, J. Chen, *Cell Res* **2018**, *28 (5)*, 507–517.
[107] H. Huang, H. Weng, W. Sun, X. Qin, H. Shi, H. Wu, B. S. Zhao, A. Mesquita, C. Liu, C. L. Yuan, Y.-C. Hu, S. Hüttelmaier, J. R. Skibbe, R. Su, X. Deng, L. Dong, M. Sun, C. Li, S. Nachtergaele, Y. Wang, C. Hu, K. Ferchen, K. D. Greis, X. Jiang, M. Wei, L. Qu, J.-L. Guan, C. He, J. Yang, J. Chen, *Nat. Cell Biol.* **2018**, *20 (3)*, 285–295.
[108] H. Song, J. Song, M. Cheng, M. Zheng, T. Wang, S. Tian, R. A. Flavell, S. Zhu, H. B. Li, C. Ding, H. Wei, R. Sun, H. Peng, Z. Tian, *Nat. Commun.* **2021**, *12 (1)*, 5522.
[109] E. Yankova, W. Blackaby, M. Albertella, J. Rak, E. De Braekeleer, G. Tsagkogeorga, E. S. Pilka, D. Aspris, D. Leggate, A. G. Hendrick, N. A. Webster, B. Andrews, R. Fosbeary, P. Guest, N. Irigoyen, M. Eleftheriou, M. Gozdecka, J. M. L. Dias, A. J. Bannister, B. Vick, I. Jeremias, G. S. Vassiliou, O. Rausch, K. Tzelepis, T. Kouzarides, *Nature* **2021**, *593 (7860)*, 597–601.
[110] A. A. Guirguis, Y. Ofir-Rosenfeld, K. Knezevic, W. Blackaby, D. Hardick, Y.-C. Chan, A. Motazedian, A. Gillespie, D. Vassiliadis, E. Y. N. Lam, K. Tran, B. Andrews, M. E. Harbour, L. Vasiliauskaite, C. J. Saunders, G. Tsagkogeorga, A. Azevedo, J. Obacz, E. S. Pilka, M. Carkill, L. MacPherson, E. N. Wainwright, B. Liddicoat, B. J. Blyth, M. R. Albertella, O. Rausch, M. A. Dawson, *Cancer Dis.* **2023**, *13 (10)*, 2228–2247.
[111] K. D. Meyer, Y. Saletore, P. Zumbo, O. Elemento, C. E. Mason, S. R. Jaffrey, *Cell* **2012**, *149 (7)*, 1635–1646.
[112] K.-J. Yoon, F. R. Ringeling, C. Vissers, F. Jacob, M. Pokrass, D. Jimenez-Cyrus, Y. Su, N.-S. Kim, Y. Zhu, L. Zheng, S. Kim, X. Wang, L. C. Doré, P. Jin, S. Regot, X. Zhuang, S. Canzar, C. He, G. Ming, H. Song, *Cell* **2017**, *171 (4)*, 877–889.e17.
[113] Y.-L. Weng, X. Wang, R. An, J. Cassin, C. Vissers, Y. Liu, Y. Liu, T. Xu, X. Wang, S. Z. H. Wong, J. Joseph, L. C. Dore, Q. Dong, W. Zheng, P. Jin, H. Wu, B. Shen, X. Zhuang, C. He, K. Liu, H. Song, G. Ming, *Neuron* **2018**, *97 (2)*, 313–325.e6.
[114] L. Xia, F. Zhang, Y. Li, Y. Mo, L. Zhang, Q. Li, M. Luo, X. Hou, Z. Du, J. Deng, E. Hao, *Front. Genet.* **2023**, *14*, 1166831.
[115] H. Huang, J. Camats-Perna, R. Medeiros, V. Anggono, J. Widagdo, *eNeuro* **2020**, *7 (5)*, ENEURO.0125–20.2020.
[116] J. Zhou, Y. Han, R. Hou, *Front Cell Dev Biol* **2023**, *11*, 1321995.

[117] X. Chen, C. Yu, M. Guo, X. Zheng, S. Ali, H. Huang, L. Zhang, S. Wang, Y. Huang, S. Qie, J. Wang, *ACS Chem. Neurosci.* **2019**, *10 (5)*, 2355–2363.
[118] Y. Geng, X. Long, Y. Zhang, Y. Wang, G. You, W. Guo, G. Zhuang, Y. Zhang, X. Cheng, Z. Yuan, J. Zan, *J. Transl. Med.* **2023**, *21 (1)*, 652.
[119] R. Yoneda, N. Ueda, R. Kurokawa, *Int. J. Mol. Sci.* **2021**, *22 (20)*, 11014.
[120] S. Zhong, H. Li, Z. Bodi, J. Button, L. Vespa, M. Herzog, R. G. Fray, *Plant Cell* **2008**, *20* (5), 1278–1288.
[121] H. Grosjean, L. Droogmans, M. Roovers, G. Keith, *Methods Enzymol.* **2007**, *425*, 55–101.
[122] S. Kellner, J. Burhenne, M. Helm, *RNA Biol.* **2010**, *7 (2)*, 237–247.
[123] A. El-Aneed, A. Cohen, J. Banoub, *Appl. Spectrosc. Rev.* **2009**, *44 (3)*, 210–230.
[124] J. B. Fenn, M. Mann, C. K. Meng, S. F. Wong, C. M. Whitehouse, *Science (1979)* **1989**, *246 (4926)*, 64–71.
[125] N. Liu, M. Parisien, Q. Dai, G. Zheng, C. He, T. Pan, *RNA* **2013**, *19 (12)*, 1848–1856.
[126] Y. T. Yu, M. D. Shu, J. A. Steitz, *RNA* **1997**, *3 (3)*, 324–331.
[127] X. Zhao, Y. T. Yu, *RNA* **2004**, *10 (6)*, 996–1002.
[128] Y. Xiao, Y. Wang, Q. Tang, L. Wei, X. Zhang, G. Jia, *Angew. Chem.* **2018**, *130 (49)*, 16227–16232.
[129] P. C. He, J. Wei, X. Dou, B. T. Harada, Z. Zhang, R. Ge, C. Liu, L. S. Zhang, X. Yu, S. Wang, R. Lyu, Z. Zou, M. Chen, C. He, *Science (1979)* **2023**, *379 (6633)*, 677–682.
[130] S. J. Emrich, W. B. Barbazuk, L. Li, P. S. Schnable, *Genome Res.* **2007**, *17 (1)*, 69–73.
[131] R. Lister, R. C. O'Malley, J. Tonti-Filippini, B. D. Gregory, C. C. Berry, A. H. Millar, J. R. Ecker, *Cell* **2008**, *133 (3)*, 523–536.
[132] J. Zhao, T. K. Ohsumi, J. T. Kung, Y. Ogawa, D. J. Grau, K. Sarma, J. J. Song, R. E. Kingston, M. Borowsky, J. T. Lee, *Mol. Cell* **2010**, *40 (6)*, 939–953.
[133] K. J. Livak, T. D. Schmittgen, *Methods* **2001**, *25 (4)*, 402–408.
[134] K. Wang, J. Peng, C. Yi, *Biochemistry* **2021**, *60 (46)*, 3410–3412.
[135] X. Jiang, B. Liu, Z. Nie, L. Duan, Q. Xiong, Z. Jin, C. Yang, Y. Chen, *Signal Transduct. Target Ther.* **2021**, *6 (1)*, 74.
[136] S. Nachtergaele, C. He, *Annu. Rev. Genet.* **2018**, *52*, 349–372.
[137] C.-M. Wei, B. Moss, *Biochemistry* **1977**, *16 (8)*, 1672–1676.
[138] R. Ge, C. Ye, Y. Peng, Q. Dai, Y. Zhao, S. Liu, P. Wang, L. Hu, C. He, *Nat. Protoc.* **2023**, *18 (2)*, 626-657.
[139] X. Yang, R. Triboulet, Q. Liu, E. Sendinc, R. I. Gregory, *Nat. Commun.* **2022**, *13 (1)*.
[140] A. V. Grozhik, B. Linder, A. O. Olarerin-George, S. R. Jaffrey, *Methods Mol. Biol.* **2017**, *1562*, 55–78.
[141] K. Chen, Z. Lu, X. Wang, Y. Fu, G.-Z. Luo, N. Liu, D. Han, D. Dominissini, Q. Dai, T. Pan, C. He, *Angew. Chem. Int. Ed.* **2015**, *54 (5)*, 1587–1590.
[142] J. Ule, K. B. Jensen, M. Ruggiu, A. Mele, A. Ule, R. B. Darnell, *Science (1979)* **2003**, *302 (5648)*, 1212–1215.
[143] M. Hafner, M. Landthaler, L. Burger, M. Khorshid, J. Hausser, P. Berninger, A. Rothballer, M. Ascano, A.-C. Jungkamp, M. Munschauer, A. Ulrich, G. S. Wardle, S. Dewell, M. Zavolan, T. Tuschl, *Cell* **2010**, *141 (1)*, 129–141.
[144] H. Lee, M. C. Schatz, *Bioinformatics* **2012**, *28 (16)*, 2097–2105.
[145] A. B. R. McIntyre, N. S. Gokhale, L. Cerchietti, S. R. Jaffrey, S. M. Horner, C. E. Mason, *Sci. Rep.* **2020**, *10 (1)*.
[146] M. Helm, F. Lyko, Y. Motorin, *Nat. Commun.* **2019**, *10 (1)*, 5669 .
[147] Z. Zhang, T. Chen, H. X. Chen, Y. Y. Xie, L. Q. Chen, Y. L. Zhao, B. Di Liu, L. Jin, W. Zhang, C. Liu, D. Z. Ma, G. S. Chai, Y. Zhang, W. S. Zhao, W. H. Ng, J. Chen, G. Jia, J. Yang, G. Z. Luo, *Nat. Methods* **2021**, *18 (10)*, 1213–1222.
[148] S. Schwartz, S. D. Agarwala, M. R. Mumbach, M. Jovanovic, P. Mertins, A. Shishkin, Y. Tabach, T. S. Mikkelsen, R. Satija, G. Ruvkun, S. A. Carr, E. S. Lander, G. R. Fink, A. Regev, *Cell* **2013**, *155 (6)*, 1409–1421.
[149] S. Liu, A. Zhu, C. He, M. Chen, *Genome Biol.* **2020**, *21 (1)*, 100.
[150] X. Wang, B. S. Zhao, I. A. Roundtree, Z. Lu, D. Han, H. Ma, X. Weng, K. Chen, H. Shi, C. He, *Cell* **2015**, *161 (6)*, 1388–1399.
[151] J. Liu, K. Li, J. Cai, M. Zhang, X. Zhang, X. Xiong, H. Meng, X. Xu, Z. Huang, J. Peng, J. Fan, C. Yi, *Mol. Cell* **2020**, *77 (2)*, 426–440.e6.
[152] B. Linder, A. V. Grozhik, A. O. Olarerin-George, C. Meydan, C. E. Mason, S. R. Jaffrey, *Nat. Methods* **2015**, *12 (8)*, 767–772.
[153] B. Molinie, J. Wang, K. S. Lim, R. Hillebrand, Z. Lu, N. Van Wittenberghe, B. D. Howard, K. Daneshvar, A. C. Mullen, P. Dedon, Y. Xing, C. C. Giallourakis, *Nat. Methods* **2016**, *13 (8)*, 692–698.
[154] C. W. Q. Koh, Y. T. Goh, W. S. S. Goh, *Nat. Commun.* **2019**, *10 (1)*, 5636.
[155] Y. Zeng, S. Wang, S. Gao, F. Soares, M. Ahmed, H. Guo, M. Wang, J. T. Hua, J. Guan, M. F. Moran, M. S. Tsao, H. H. He, *PLoS Biol.* **2018**, *16 (9)*, e2006092.
[156] Z. Guo, A. M. Shafik, P. Jin, H. Wu, *Bioinformatics* **2022**, *38 (20)*, 4705–4712.
[157] Z. Zhang, T. Chen, H.-X. Chen, Y.-Y. Xie, L.-Q. Chen, Y.-L. Zhao, B.-D. Liu, L. Jin, W. Zhang, C. Liu, D.-Z. Ma, G.-S. Chai, Y. Zhang, W.-S. Zhao, W. H. Ng, J. Chen, G. Jia, J. Yang, G.-Z. Luo, *Nat. Methods* **2021**, *18 (10)*, 1213–1222.
[158] Y. Wang, Y. Xiao, S. Dong, Q. Yu, G. Jia, *Nat. Chem. Biol.* **2020**, *16 (8)*, 896–903.
[159] X. Shu, J. Cao, M. Cheng, S. Xiang, M. Gao, T. Li, X. Ying, F. Wang, Y. Yue, Z. Lu, Q. Dai, X. Cui, L. Ma, Y. Wang, C. He, X. Feng, J. Liu, *Nat. Chem. Biol.* **2020**, *16 (8)*, 887–895.
[160] X. Shu, Q. Dai, T. Wu, I. R. Bothwell, Y. Yue, Z. Zhang, J. Cao, Q. Fei, M. Luo, C. He, J. Liu, *J. Am. Chem. Soc.* **2017**, *139 (48)*, 17213–17216.
[161] Z. Zhang, L.-Q. Chen, Y.-L. Zhao, C.-G. Yang, I. A. Roundtree, Z. Zhang, J. Ren, W. Xie, C. He, G.-Z. Luo, *Sci. Adv.* **2019**, *5 (7)*, eaax0250.
[162] M. A. Garcia-Campos, S. Edelheit, U. Toth, M. Safra, R. Shachar, S. Viukov, R. Winkler, R. Nir, L. Lasman, A. Brandis, J. H. Hanna, W. Rossmanith, S. Schwartz, *Cell* **2019**, *178 (3)*, 731–747.e16.
[163] M. Imanishi, S. Tsuji, A. Suda, S. Futaki, *Chem. Commun.* **2017**, *53 (96)*, 12930–12933.
[164] K. D. Meyer, *Nat. Methods* **2019**, *16 (12)*, 1275–1280.
[165] M. Tegowski, M. N. Flamand, K. D. Meyer, *Mol. Cell* **2022**, *82 (4)*, 868–878.e10.
[166] S. Picelli, O. R. Faridani, Å. K. Björklund, G. Winberg, S. Sagasser, R. Sandberg, *Nat. Protoc.* **2014**, *9 (1)*, 171–181.
[167] G. X. Y. Zheng, J. M. Terry, P. Belgrader, P. Ryvkin, Z. W. Bent, R. Wilson, S. B. Ziraldo, T. D. Wheeler, G. P. McDermott, J. Zhu, M. T. Gregory, J. Shuga, L. Montesclaros, J. G. Underwood, D. A. Masquelier, S. Y. Nishimura, M. Schnall-Levin, P. W. Wyatt, C. M. Hindson, R. Bharadwaj, A. Wong, K. D. Ness, L. W. Beppu, H. J. Deeg, C. McFarland, K. R. Loeb, W. J. Valente, N. G. Ericson, E. A. Stevens, J. P. Radich, T. S. Mikkelsen, B. J. Hindson, J. H. Bielas, *Nat. Commun.* **2017**, *8 (1)*, 14049.
[168] *Chromium Next GEM Single Cell 3′ Reagent Kits v3.1*; **2019**. www.10xgenomics.com/trademarks.

[169] H. C. O'Farrell, F. N. Musayev, J. N. Scarsdale, J. P. Rife, *Biochemistry* **2010**, *49 (12)*, 2697–2704.
[170] H. C. O'Farrell, N. Pulicherla, P. M. Desai, J. P. Rife, *RNA* **2006**, *12 (5)*, 725–733.
[171] F. Zhuang, R. T. Fuchs, Z. Sun, Y. Zheng, G. B. Robb, *Nucleic Acids Res.* **2012**, *40 (7)*, e54–e54.
[172] M. Frommer, L. E. McDonald, D. S. Millar, C. M. Collis, F. Watt, G. W. Grigg, P. L. Molloy, C. L. Paul, *Proc. Natl. Acad. Sci. USA* **1992**, *89 (5)*, 1827–1831.
[173] D. J. Wright, C. R. Force, B. M. Znosko, *Nucleic Acids Res.* **2018**, *46 (22)*, 12099–12108.
[174] M. S. Packer, D. R. Liu, *Nat. Rev. Genet.* **2015**, *16 (7)*, 379–394.
[175] J. Grünewald, R. Zhou, S. P. Garcia, S. Iyer, C. A. Lareau, M. J. Aryee, J. K. Joung, *Nature* **2019**, *569 (7756)*, 433–437.
[176] N. M. Gaudelli, D. K. Lam, H. A. Rees, N. M. Solá-Esteves, L. A. Barrera, D. A. Born, A. Edwards, J. M. Gehrke, S.-J. Lee, A. J. Liquori, R. Murray, M. S. Packer, C. Rinaldi, I. M. Slaymaker, J. Yen, L. E. Young, G. Ciaramella, *Nat. Biotechnol.* **2020**, *38 (7)*, 892–900.
[177] N. M. Gaudelli, A. C. Komor, H. A. Rees, M. S. Packer, A. H. Badran, D. I. Bryson, D. R. Liu, *Nature* **2017**, *551 (7681)*, 464–471.
[178] X.-M. Liu, J. Zhou, Y. Mao, Q. Ji, S.-B. Qian, *Nat. Chem. Biol.* **2019**, *15 (9)*, 865–871.
[179] C. Wilson, P. J. Chen, Z. Miao, D. R. Liu, *Nat. Biotechnol.* **2020**, *38 (12)*, 1431–1440.
[180] H. Shi, Y. Xu, N. Tian, M. Yang, F.-S. Liang, *Nat. Commun.* **2022**, *13 (1)*, 1958.
[181] Y.-L. Xiao, Y. Wu, W. Tang, *Nat. Biotechnol.* **2024**, doi: 10.1038/s41587-023-01994-3.
[182] H. Yao, C.-C. Gao, D. Zhang, J. Xu, G. Song, X. Fan, D.-B. Liang, Y.-S. Chen, Q. Li, Y. Guo, Y.-T. Cai, L. Hu, Y.-L. Zhao, Y.-P. Sun, Y. Yang, J. Han, Y.-G. Yang, *Nat. Commun.* **2023**, *14 (1)*, 315.
[183] Y. Li, Y. Wang, M. Vera-Rodriguez, L. C. Lindeman, L. E. Skuggen, E. M. K. Rasmussen, I. Jermstad, S. Khan, M. Fosslie, T. Skuland, M. Indahl, S. Khodeer, E. K. Klemsdal, K. X. Jin, K. T. Dalen, P. Fedorcsak, G. D. Greggains, M. Lerdrup, A. Klungland, K. F. Au, J. A. Dahl, *Nat. Biotechnol.* **2023**, doi: 10.1038/s41587-023-01831-7
[184] K. Hamashima, K. W. Wong, T. W. Sam, J. H. J. Teo, R. Taneja, M. T. N. Le, Q.-J. Li, J. H. Hanna, H. Li, Y.-H. Loh, *Mol. Cell* **2023**, *83 (17)*, 3205–3216.e5.
[185] M. Bartosovic, M. Kabbe, G. Castelo-Branco, *Nat. Biotechnol.* **2021**, *39 (7)*, 825–835.
[186] H. S. Kaya-Okur, S. J. Wu, C. A. Codomo, E. S. Pledger, T. D. Bryson, J. G. Henikoff, K. Ahmad, S. Henikoff, *Nat. Commun.* **2019**, *10 (1)*, 1930.
[187] P. J. Skene, S. Henikoff, *eLife* **2017**, *16 (6)*, e21856.
[188] L. Di, Y. Fu, Y. Sun, J. Li, L. Liu, J. Yao, G. Wang, Y. Wu, K. Lao, R. W. Lee, G. Zheng, J. Xu, J. Oh, D. Wang, X. S. Xie, Y. Huang, J. Wang, *Proc. Natl. Acad. Sci. U.S.A.* **2020**, *117 (6)*, 2886–2893.
[189] B. Lu, L. Dong, D. Yi, M. Zhang, C. Zhu, X. Li, C. Yi, *eLife* **2020**, *9*, 1–16.
[190] L. Liu, C. Liu, A. Quintero, L. Wu, Y. Yuan, M. Wang, M. Cheng, L. Leng, L. Xu, G. Dong, R. Li, Y. Liu, X. Wei, J. Xu, X. Chen, H. Lu, D. Chen, Q. Wang, Q. Zhou, X. Lin, G. Li, S. Liu, Q. Wang, H. Wang, J. L. Fink, Z. Gao, X. Liu, Y. Hou, S. Zhu, H. Yang, Y. Ye, G. Lin, F. Chen, C. Herrmann, R. Eils, Z. Shang, X. Xu, *Nat. Commun.* **2019**, *10*, 470.
[191] *Chromium Next GEM Single Cell Multiome ATAC + Gene Expression Reagent Kits User Guide,* **2022**, 10x Genomics. https://cdn.10xgenomics.com/image/upload/v1666737555/support-documents/CG000338_ChromiumNextGEM_Multiome_ATAC_GEX_User_Guide_RevF.pdf.
[192] J. Cao, J. S. Packer, V. Ramani, D. A. Cusanovich, C. Huynh, R. Daza, X. Qiu, C. Lee, S. N. Furlan, F. J. Steemers, A. Adey, R. H. Waterston, C. Trapnell, J. Shendure, *Science* **2017**, *357 (6352)*, 661–667.
[193] Rosenberg, A. B.; Charles, †; Roco, M.; Muscat, R. A.; Kuchina, A.; Sample, P.; Yao, Z.; Graybuck, L. T.; Peeler, D. J.; Mukherjee, S.; Chen, W.; Pun, S. H.; Sellers, D. L.; Tasic, B.; Seelig, G. *Science* **2018**, *360 (6385)*, 176–182.
[194] H. Satam, K. Joshi, U. Mangrolia, S. Waghoo, G. Zaidi, S. Rawool, R. P. Thakare, S. Banday, A. K. Mishra, G. Das, S. K. Malonia, *Biology (Basel)* **2023**, *12 (7)*, 997.
[195] D. R. Garalde, E. A. Snell, D. Jachimowicz, B. Sipos, J. H. Lloyd, M. Bruce, N. Pantic, T. Admassu, P. James, A. Warland, M. Jordan, J. Ciccone, S. Serra, J. Keenan, S. Martin, L. McNeill, E. J. Wallace, L. Jayasinghe, C. Wright, J. Blasco, S. Young, D. Brocklebank, S. Juul, J. Clarke, A. J. Heron, D. J. Turner, *Nat. Methods* **2018**, *15 (3)*, 201–206.
[196] I. Anreiter, Q. Mir, J. T. Simpson, S. C. Janga, M. Soller, *Trends Biotechnol.* **2021**, *39 (1)*, 72–89.
[197] A. M. Price, K. E. Hayer, A. B. R. McIntyre, N. S. Gokhale, J. S. Abebe, A. N. Della Fera, C. E. Mason, S. M. Horner, A. C. Wilson, D. P. Depledge, M. D. Weitzman, *Nat. Commun.* **2020**, *11 (1)*, 6016.
[198] A. Leger, P. P. Amaral, L. Pandolfini, C. Capitanchik, F. Capraro, V. Miano, V. Migliori, P. Toolan-Kerr, T. Sideri, A. J. Enright, K. Tzelepis, F. J. van Werven, N. M. Luscombe, I. Barbieri, J. Ule, T. Fitzgerald, E. Birney, T. Leonardi, T. Kouzarides, *Nat. Commun.* **2021**, *12 (1)*, 7198.
[199] P. Jenjaroenpun, T. Wongsurawat, T. D. Wadley, T. M. Wassenaar, J. Liu, Q. Dai, V. Wanchai, N. S. Akel, A. Jamshidi-Parsian, A. T. Franco, G. Boysen, M. L. Jennings, D. W. Ussery, C. He, I. Nookaew, *Nucleic Acids Res.* **2021**, *49 (2)*, e7–e7.
[200] P. N. Pratanwanich, F. Yao, Y. Chen, C. W. Q. Koh, Y. K. Wan, C. Hendra, P. Poon, Y. T. Goh, P. M. L. Yap, J. Y. Chooi, W. J. Chng, S. B. Ng, A. Thiery, W. S. S. Goh, J. Göke, *Nat. Biotechnol.* **2021**, *39 (11)*, 1394–1402.
[201] H. Liu, O. Begik, M. C. Lucas, J. M. Ramirez, C. E. Mason, D. Wiener, S. Schwartz, J. S. Mattick, M. A. Smith, E. M. Novoa, *Nat. Commun.* **2019**, *10 (1)*, 4079.
[202] D. A. Lorenz, S. Sathe, J. M. Einstein, G. W. Yeo, *RNA* **2020**, *26 (1)*, 19–28.
[203] Y. Gao, X. Liu, B. Wu, H. Wang, F. Xi, M. V. Kohnen, A. S. N. Reddy, L. Gu, *Genome Biol.* **2021**, *22 (1)*, 22.
[204] C. Hendra, P. N. Pratanwanich, Y. K. Wan, W. S. S. Goh, A. Thiery, J. Göke, *Nat. Methods* **2022**, *19 (12)*, 1590–1598.
[205] E. Sendinc, Y. Shi, *Mol. Cell* **2023**, *83 (3)*, 428–441.

Manuscript received: December 30, 2023
Revised manuscript received: February 24, 2024
Version of record online: ■■, ■■

REVIEW

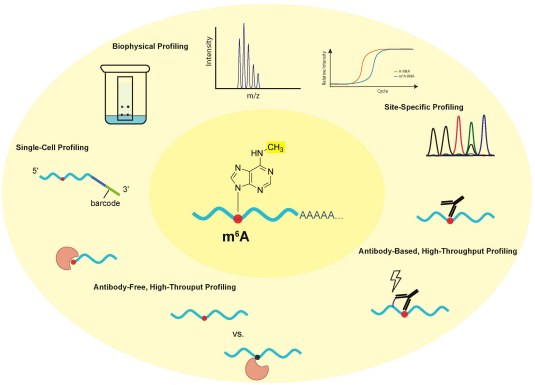

*R. Ge, M. E. He, W. Tang**

1 – 20

N^6-methyladenosine in Mammalian Messenger RNA: Function, Location, and Quantitation